Chromosomes and Gene Expression

Chromosome Structure II: Stem-loops and Circle-loops

Reviewed Preprint
v2 • June 20, 2024
Revised by authors

Reviewed Preprint
v1 • February 5, 2024

Wenfan Ke, Miki Fujioka, Paul Schedl, James B. Jaynes

Department of Molecular Biology, Princeton University, Princeton NJ 08544 • Department of Biochemistry and Molecular Biology, Thomas Jefferson University, Philadelphia, PA 19107

https://en.wikipedia.org/wiki/Open_access
Copyright information

Abstract

The chromosomes in multicellular eukaryotes are organized into a series of topologically independent loops called TADs. In flies, TADs are formed by physical interactions between neighboring boundaries. Fly boundaries exhibit distinct partner preferences, and pairing interactions between boundaries are typically orientation-dependent. Pairing can be head-to-tail or head-to-head. The former generates a stem-loop TAD, while the latter gives a circle-loop TAD. The TAD that encompasses the *Drosophila even skipped* (*eve*) gene is formed by the head-to-tail pairing of the *nhomie* and *homie* boundaries. To explore the relationship between loop topology and the physical and regulatory landscape, we flanked the *nhomie* boundary region with two attP sites. The attP sites were then used to generate four boundary replacements: *λ DNA*, *nhomie forward* (WT orientation), *nhomie reverse* (opposite of WT orientation), and *homie forward* (same orientation as WT *homie*). The *nhomie forward* replacement restores the WT physical and regulatory landscape: In MicroC experiments, the *eve* TAD is a “volcano” triangle topped by a plume, and the *eve* gene and its regulatory elements are sequestered from interactions with neighbors. The *λ DNA* replacement lacks boundary function: the endpoint of the “new” *eve* TAD on the *nhomie* side is ill-defined, and *eve* stripe enhancers activate a nearby gene, *eIF3j*. While *nhomie reverse* and *homie forward* restore the *eve* TAD, the topology is a circle-loop, and this changes the local physical and regulatory landscape. In MicroC experiments, the *eve* TAD interacts with its neighbors, and the plume at the top of the *eve* triangle peak is instead flanked by a pair of “clouds” of contacts with the next-door TADs. Consistent with the loss of isolation afforded by the stem-loop topology, the *eve* enhancers weakly activate genes in the neighboring TADs. Conversely, *eve* function is partially disrupted.

eLife assessment

This **valuable** work investigates the role of boundary elements in the formation of 3D genome architecture. The authors established a specific model system that allowed them to manipulate boundary elements and examine the resulting genome topology. The work yielded the first demonstration of the existence of stem and circle loops in a genome and confirms a model which had been posited based on extensive prior genetic work, providing insights into how 3D genome topologies affect enhancer-promoter communication. The evidence is **solid**, although the degree of generalization remains uncertain.

https://doi.org/10.7554/eLife.94114.2.sa2

Introduction

Chromosomes in multicellular animals are organized into a series of topologically independent looped domains, called TADs, or topologically associating domains (Cavalheiro et al. 2021; Chetverina et al. 2017; Jerković et al. 2020; Matthews and White 2019; Rowley and Corces 2018). The arrangement of TADs in a given chromosomal DNA segment is generally (though not precisely) similar in different tissues and developmental stages, and this is a reflection of the mechanism underlying TAD formation—the endpoints of TADs are determined by a special class of elements called chromatin boundaries or insulators. While boundary-like elements have been identified in a wide range of animals and plants, the properties of this class of DNA elements have been most fully characterized in *Drosophila* (Cavalheiro et al. 2021; Chetverina et al. 2017). Fly boundaries have one or more large (100-400 bp) nucleosome-free nuclease-hypersensitive sequences that are targets for multiple DNA binding chromosomal architectural proteins. While only a single chromosomal architectural protein, CTCF, has been characterized in mammals, there are several dozen such proteins in flies, and the list is still growing (Heger et al. 2013; Heger and Wiehe 2014; Schoborg and Labrador 2010). In addition to subdividing the chromosome into a series of loops, fly boundary elements have insulating activity. When placed between enhancers or silencers and their target promoters, boundaries block regulatory interactions (Bell et al. 2001; Chetverina et al. 2014; Chetverina et al. 2017). This activity provides a mechanism for delimiting units of independent gene activity: genes located between a pair of compatible boundaries are subject to regulatory interactions with enhancers/silencers present in the same chromosomal interval, while they are insulated from the effects of enhancers/silencers located beyond either boundary in adjacent regulatory neighborhoods. It is currently thought that their ability to organize the chromosome into topologically independent loops is important for their insulating activity (Cai and Shen 2001; Gohl et al. 2011; Muravyova et al. 2001).

Studies dating back to the 1990's have suggested that fly boundaries subdivide the chromosome into loops by physically pairing with each other (Chetverina et al. 2014; Chetverina et al. 2017). In these first experiments, regulatory interactions were observed for transgenes inserted at distant sites in chromosome that were carrying either the *gypsy* transposon boundary *su(Hw)* or the bithorax complex (BX-C) boundary *Mcp* (Muller et al. 1999; Sigrist and Pirrotta 1997; Vazquez et al. 1993). Further support for the idea that boundaries function by pairing has come from chromatin immunoprecipitation, chromosome conformation capture (CCC), MicroC, and direct imaging experiments (Chen et al. 2018; Li et al. 2011; Vazquez et al. 2006). More recent studies have revealed physical interactions in the CNS, such as those found for *su(Hw)* and

Mcp, which "reach over" multiple intervening TADs, consistent with them playing an important role in cell type-specific gene regulation (Mohana et al. 2023) by bringing distant enhancers and promoters together.

The parameters governing pairing interactions have been defined using insulator bypass, transvection and boundary competition assays. These studies have shown that fly boundaries are able to pair not only with heterologous boundaries but also with copies of themselves. Moreover, the pairing interactions typically exhibit a number of characteristic features: promiscuity coupled with clear partner preferences, and orientation dependence.

Partner preferences depend upon the chromosomal architectural proteins that interact with each boundary. For example, in the boundary bypass assay, a set of enhancers are placed upstream of two reporters (Cai and Shen 2001; Kyrchanova et al. 2008a; Muravyova et al. 2001). When multimerized CTCF sites are placed between the enhancers and the closest reporters, both reporters are insulated from the enhancers. When a second set of multimerized dCTCF sites are placed downstream of the closest reporter, bypass is observed. In this case the closest reporter, which is bracketed by the multimerized dCTCF sites, is still insulated from the enhancers; however, the downstream reporter is activated (Muravyova et al. 2001). Heterologous combinations give a different result: when multimerized dCTCF sites are placed upstream of the closest reporter and multimerized Zw5 sites are placed downstream, no bypass is observed. Endogenous fly boundaries also show partner preferences in bypass assays and in boundary competition experiments (Gohl et al. 2011; Kyrchanova et al. 2011; Kyrchanova et al. 2008b). On the other hand, while boundaries have partner preferences, they are also promiscuous in their ability to establish functional interactions with other boundaries. For example, the *Fab-8* insulator can partner with *scs'* from the *Drosophila* heat shock locus (Gohl et al. 2011).

In addition, to partner preferences, pairing interactions between endogenous fly boundaries are, with a few exceptions, orientation-dependent. Self-pairing interactions are head-to-head. This seems to be a common feature of fly boundaries and has been observed for *scs*, *scs'*, *iA2*, *wari*, *Mcp*, *Fab-8*, *AB-I, homie* and *nhomie* (Fujioka et al. 2016; Kyrchanova et al. 2008a). In contrast, pairing interactions between heterologous boundaries can be head-to-head or head-to-tail. The two boundaries bracketing the *even-skipped* (*eve*) locus, *homie* and *nhomie*, pair with each other head-to-tail, while boundaries in the *Abdominal-B* (*Abd-B*) region of BX-C usually pair with their neighbors head-to-head. The topology of the loops (TADs) generated by head-to-tail and head-to-head pairing in *cis* between neighboring boundaries is distinct. As illustrated in **Fig. 1**, head-to-tail pairing generates stem-loops, while head-to-head pairing generates circle-loops. The loops could be connected to each other by unanchored loops (**Fig. 1A** and C), or they could be linked directly to each other if boundaries can pair simultaneously with both neighbors (**Fig. 1B** and D). An alternating pattern of TADs connected by DNA segments that crosslink to each other with reduced frequency (c.f., *λ DNA* below) is not often observed in MicroC experiments. Instead, most TADs appeared to be directly connected to both of their neighbors without an intervening unanchored loop (Batut et al. 2022; Bing et al. 2024; Levo et al. 2022), (see also below). This would suggest that TAD boundaries are typically linked to both neighbors, either simultaneously or as alternating pair-wise interactions.

Key to understanding the 3D organization of chromosomes in multicellular eukaryotes will be the identification of TADs that are stem-loops and TADs that are circle-loops. In the studies reported here, we have used MicroC to analyze the contact maps generated by stem-loops and circle-loops. Stem-loop and circle-loop TADs are expected to interact differently with their neighbors, and this should be reflected in the patterns of crosslinking events between neighboring TADs. As illustrated for linked stem-loops in **Fig. 1B**, TAD2 is isolated from its next-door neighbors, TAD1 and TAD3. In this configuration, crosslinking events between sequences in TAD2 and sequences in TAD1 and TAD3 will be suppressed. On the other hand, TAD1 and TAD3 are in comparatively close proximity, and crosslinking between sequences in these two TADs is expected to be enhanced. A different

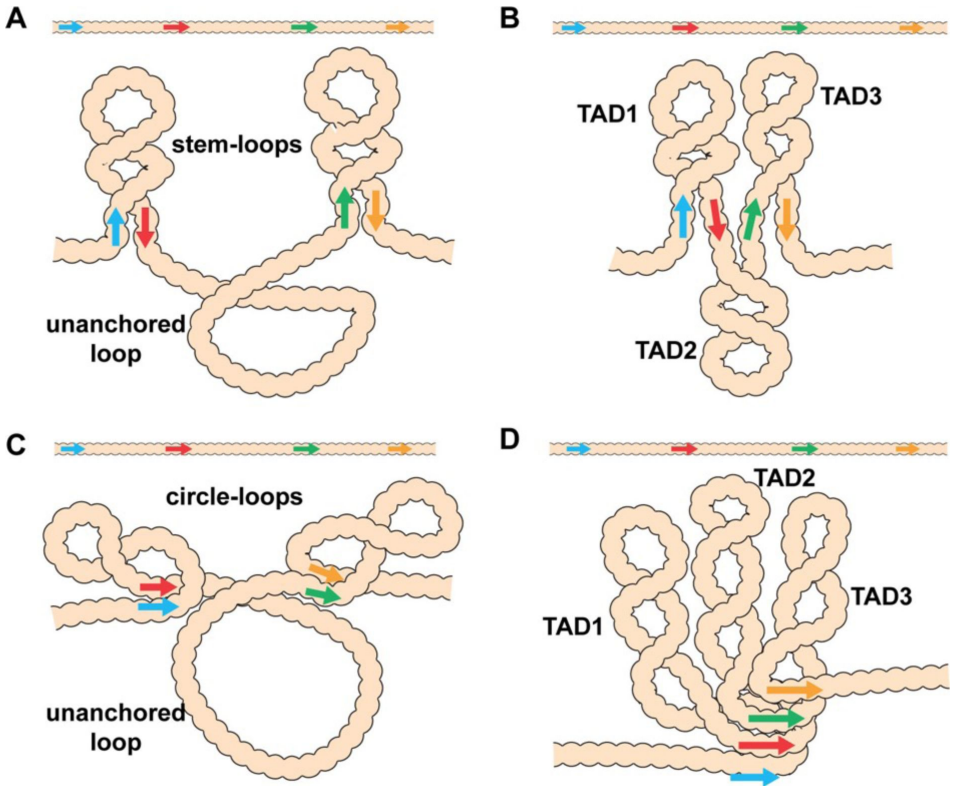

Figure 1.

Diagram of the possible loop topologies generated by head-to-head and head-to-tail pairing.

A) Head-to-tail boundary pairing (arrows) generates a series of stem-loops linked together by an unanchored loop. In this case, the main axis of the chromosome would correspond to the unanchored loops connecting different stem-loops. B) If boundaries pair with both neighbors (head-to-tail), the stem-loops would be linked to each other by the paired boundaries. In this case the main axis of the chromosome will correspond to the paired boundaries. C) Head-to-head boundary pairing generates a series of circle-loops linked together by an unanchored loop. The unanchored loop will be the main axis of the chromosome. D) If boundaries pair with both neighbors (head-to-head), the chromatin fiber will be organized into a series of circle-loops connected to each other at their base, and these paired boundaries will define the chromosomal axis. In both B) and D), the pairing interactions between the blue and red boundaries need not be in register with the pairing of the red boundary to the next-door green boundary. In this case, the main axis of the chromosome may bend and twist, and this could impact the relative orientation of the stem-loops/circle-loops. More complex structures would be generated by mixtures of stem-loops and circle-loops.

pattern of neighborly interactions is expected for circle-loop TADs. In this case, the TAD in the middle, TAD2, is expected to interact with both of its neighbors (**Fig. 1D**). To test these predictions, we have first compared the MicroC contact profiles for stem-loop and circle-loop TADs. For stem-loops we selected the *eve* TAD, while for circle-loops we chose the four TADs that comprise the *Abd-B* parasegment-specific regulatory domains. We show that these stem-loop and circle-loop TADs have distinctive crosslinking signatures. To confirm these MicroC signatures, we converted the topology of the *eve* TAD from a stem-loop to a circle-loop. In addition to changing the MicroC signature of the *eve* TAD, the change in topology is accompanied by changes in the regulatory interactions between *eve* and its neighbors.

Results

Stem-loops versus circle-loops

The distinctive loop topologies of stem-loops and circle-loops are expected to be reflected in the contact maps that are generated in MicroC experiments. To determine if this is the case, we compared the MicroC contact maps for the *eve* TAD and the TADs that correspond to the four *Abd-B* parasegment specific regulatory domains, *iab-5*, *iab-6*, *iab-7* and *iab-8*. The *eve* TAD is generated by pairing interactions between the *nhomie* boundary upstream of the *eve* transcription unit and the *homie* boundary downstream. Since *nhomie* and *homie* pair with each other head-to-tail, the *eve* TAD has a stem-loop topology (Fujioka et al. 2016). Unlike the *eve* boundaries, the boundaries that delimit the *Abd-B* regulatory domains are thought to pair with their neighbors head-to-head (Chetverina et al. 2017; Kyrchanova et al. 2008a; Kyrchanova et al. 2011; Kyrchanova et al. 2008b). This means that the parasegment-specific regulatory domain TADs, *iab-5*, *iab-6*, *iab-7* and *iab-8*, are expected to have a circle-loop topology.

As shown in **Fig. 2**, the *eve* TAD and the four *Abd-B* TADs have distinctive MicroC contact patterns. The *eve* TAD is a “volcano” triangle with a plume. The endpoints of the volcano triangle are delimited by *nhomie* on the left and *homie* on the right, and within the *eve* locus (the volcano), there are additional enhanced interactions. While the volcano triangle is generated by contacts between sequences within the *eve* stem-loop, contacts between sequences in *eve* and in the neighboring TAD on the left, TL (which contains multiple sub-TADs and six genes: *CG15863*, *CG1418*, *Pal1*, *CG12133*, *eIF3j* and *CG12134*), are much reduced (L-ev in **Fig 2A**). There is a similar suppression of contacts between sequences in the *eve* TAD and sequences in the large neighboring TAD on the right, TM (which contains *TER94* and *Pka-R2*) (ev-M in **Fig. 2A**). On the other hand, as expected from the regulatory interactions observed for stem-loops in boundary bypass experiments (Kyrchanova et al. 2008a), physical contacts between sequences in TL and TM are enhanced compared to those between *eve* and TL (L-ev) or TM (ev-M). Because of the preferential interactions between TADs to either side of the *eve* stem-loop, the *eve* volcano triangle is topped by a plume (L-M in **Fig. 2A**). TM also interacts with the two TADs farther to the left of *eve*, TK (K-M in **Fig. 2A**) and TJ (J-M in **Fig. 2A**) (see also **Fig. Supplemental 1**).

Like the *eve* boundaries, the TADs in the *Abd-B* region of BX-C region are connected to their neighbors by the boundaries at their base. As predicted from genetic studies on BX-C boundaries, each TAD corresponds to one of the four parasegment-specific regulatory domains. While the MicroC contact maps for the four *Abd-B* TADs resemble the contact patterns in the *eve* TAD, these *Abd-B* TADs differ from *eve* in that there are no plumes above their triangle peaks (**Fig. 2B**). Instead, the *Abd-B* TADs are overlaid by a series of rectangular interlocking low-density contact (LDC) domains, or clouds. As illustrated in **Fig 2B**, the *iab-6* regulatory domain is flanked by clouds generated by crosslinking with its next door neighbors *iab-5* (5-6) and *iab-7*(6-7), followed by crosslinking with neighbors that are a TAD away from *iab-6*, *iab-4* (4-6) and *iab-8* (6-8). The other regulatory domains also form a unique set of interlocking LDCs/clouds with their immediate neighbors, their next-next door neighbors, and their next-next-next door neighbors.

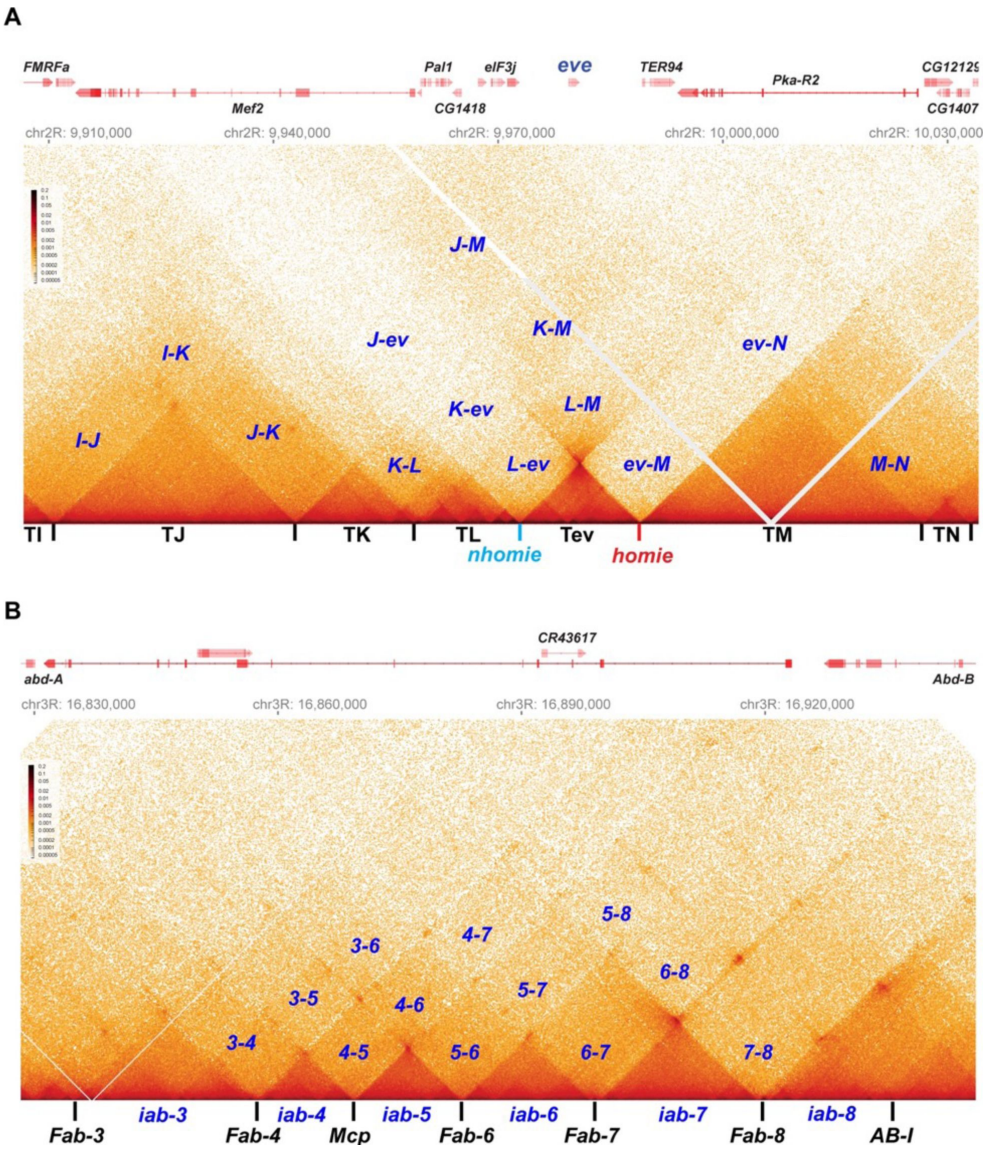

Figure 2.

Stem-loops and circle-loops.

"*Once in a while you get shown the light in the strangest of places if you look at it right*."[a] MicroC contact profile for *Drosophila* wild-type (*yw*) NC14 embryos. The bin size for each panel is 200 bp. A) *eve* and neighboring TADs (TI, TJ, TK TL, TM and TN). The *eve* TAD is a volcano with a plume that is anchored by *nhomie* (*nh*) and *homie* (*h*). The plume is generated by crosslinking of sequences in the two neighboring TADs. At the bottom of the plume, TL sequences are linked to sequences in TM close to *eve*, including *TER94*. At the next level, sequences in TK are linked to TM (region K-M). In addition, sequences in TL are linked to sequences in TM located beyond the *TER94* gene. At the next level, sequences in TJ are linked to sequences in TM. Note that interactions between sequences in TL and TJ and sequences in TM close to the *eve* TAD are somewhat less frequent than those farther away from the *eve* TAD. Sequences in the neighboring TADs also interact with each other, as indicated. For example, sequences in TK and TJ interact with each other (J-K) and also interact with sequences in TI (I-K and I-J). B) The Bithorax *Abd-B* gene and the parasegment-(PS-) specific regulatory domains *iab-3, iab-4*, *iab-5*, *iab-6*, *iab-7*, and *iab-8*. *iab-4* regulates the *abd-A* gene in PS9, while *iab-5* – *iab-8* regulate *Abd-B* in PSs 10 – 13, respectively. These domains are separated from each other by the boundary elements *Fab-4*, *Mcp*, *Fab-6*, *Fab-7*, and *Fab-8*, as indicated. The *AB-I* boundary is located upstream of the *Abd-B* promoter. Each regulatory domain corresponds to a TAD. Though partially insulated from each other, each TAD interacts with its immediate neighbors. For example, *iab-5* interacts with its immediate neighbors *iab-4* and *iab-6* to give *4-5* and *5-6* respectively. It also interacts with the next-next door neighbor *iab-7* (*5-7*) and even its next-next-next door neighbor *iab-8* (*5-8*). ([a] from "Scarlet Begonias" by the Grateful Dead, ©1974).

TAD formation in a nhomie deletion

To further investigate the pairing properties and functioning of the *eve* boundaries, we used CRISPR-Cas9 to add two attP sites flanking the *nhomie* region, replacing the region with a mini-*white* gene. Using mini-*white* as an exchange maker, ΦC31 recombinase-mediated cassette exchange (RMCE) was used to restore the sequence of the region, with *nhomie* modifications. As a control for possible effects of the sequences introduced in generating the modification, we reinserted a 597 bp *nhomie* DNA fragment in the same orientation as the endogenous *nhomie* boundary (*nhomie forward*). To maintain roughly the same distance between *eve* and the neighboring TAD in the *nhomie* deletion, we introduced a 606 bp DNA fragment from phage 11 (*λ DNA*). **Fig. 3** (and **Fig. Supplemental 1**) shows the MicroC contact profiles for the *nhomie forward* and *λ DNA* replacements in 12-16 hr embryos (mid-embryogenesis: stages 12-14). Except that the sequencing depth of the *nhomie forward* replacement is not as great as the WT shown for the *eve* locus in **Fig. 2**, the profile is quite similar. Like WT, there are sub-TADs within the *eve* TAD. One of these appears to link *homie* and the neighboring PRE to the *eve* promoter-proximal PRE (Fujioka et al. 2008), and is marked by an interaction dot (asterisk in **Fig. 3A**). Another links *nhomie* to the *eve* promoter region (blue arrow in **Fig. 3A**). The *eve* TAD is topped by a plume which is generated by interactions between sequences in neighboring TADs TL with TM (L-M). On the other hand, interactions between *eve* and its neighbors are suppressed. Like *eve*, there are sub-TADs in the neighboring TAD, TL. The TL sub-TAD closest to *eve* (TL4) corresponds to the *CG12134* transcription unit (green arrowhead marks the boundary: **Fig. 3**), while the neighboring sub-TAD (TL3) encompasses the *eIF3j* transcription unit (blue arrowhead: **Fig. 3**).

The MicroC profile of the *λ DNA* replacement (**Fig. 3D**) is quite different from that of either *nhomie forward* or WT, which are similar (**Figs. 2A** and **3A**). While *homie* still defines the distal (relative to the centromere) end of the *eve* locus, the *λ DNA* replacement does not function as a TAD boundary, and the leftward endpoint of the *eve* TAD is no longer well-defined. One new "endpoint" for the *eve* locus maps to sequences between *CG12134* and *eIF3j* (green arrowhead), which in wild type corresponds to the left boundary of the TL sub-TAD TL4. The other endpoint maps to sequences between *eIF3j* and *CG12133* (blue arrowhead), which in wild type define the left boundary of the TL sub-TAD TL3. These interactions are not as stable as those between *nhomie* and *homie*, as the density of interaction dots is lower. Furthermore, they appear to flip back and forth between alternative endpoints (as indicated by the green and blue double arrows in **Fig. 3F**) based on the MicroC contact profile, which is consistent with a mixture of (at least) two conformations. The *eve* TAD also interacts with sequences in the two other TL sub-TADs, TL1 and TL2. In addition, the *eve* promoter appears to interact with sequences located upstream of *CG12134* (purple arrowhead in **Fig. 3D** and double arrow in **Fig. 3F**), while this interaction is not observed in the *nhomie forward* replacement. While the TL TAD (from the TK:TL boundary to *nhomie*) is also disrupted by the *nhomie* deletion (it has a much less distinct "volcano apex", and its right-most sub-TAD TL4 is now fused with the *eve* TAD), the left-most TL sub-TADs (TL1, TL2, and TL3) are still present, indicating that their formation does not depend on *nhomie*. As shown in the virtual 4C at *homie* viewpoint in **Fig. 3B** and **Fig. 3E**, the *homie* boundary interacts with the *nhomie forward* replacement, but does not contact the *λ DNA* replacement.

eve enhancers activate *eIF3j* expression in the *nhomie* deletion

In transgene assays, boundary elements block regulatory interactions when interposed been enhancers (or silencers) and reporter genes (Chetverina et al. 2014; Chetverina et al. 2017; Kellum and Schedl 1992). To determine whether this is also true in their endogenous context, we compared the expression in syncytial blastoderm embryos of the two genes that flank *nhomie* at the *eve* locus, *eIF3j* and *CG12134*. As the *nhomie* deletion eliminates *homie*'s pairing partner and disrupts the *eve* TAD, we also examined the expression of *eve* and of the gene just beyond the *homie* boundary, *TER94*, which has strong maternal expression through stage 11 (**Fig. Supplemental 3B**, WT). Consistent with the seemingly normal MicroC profile on the *homie* side

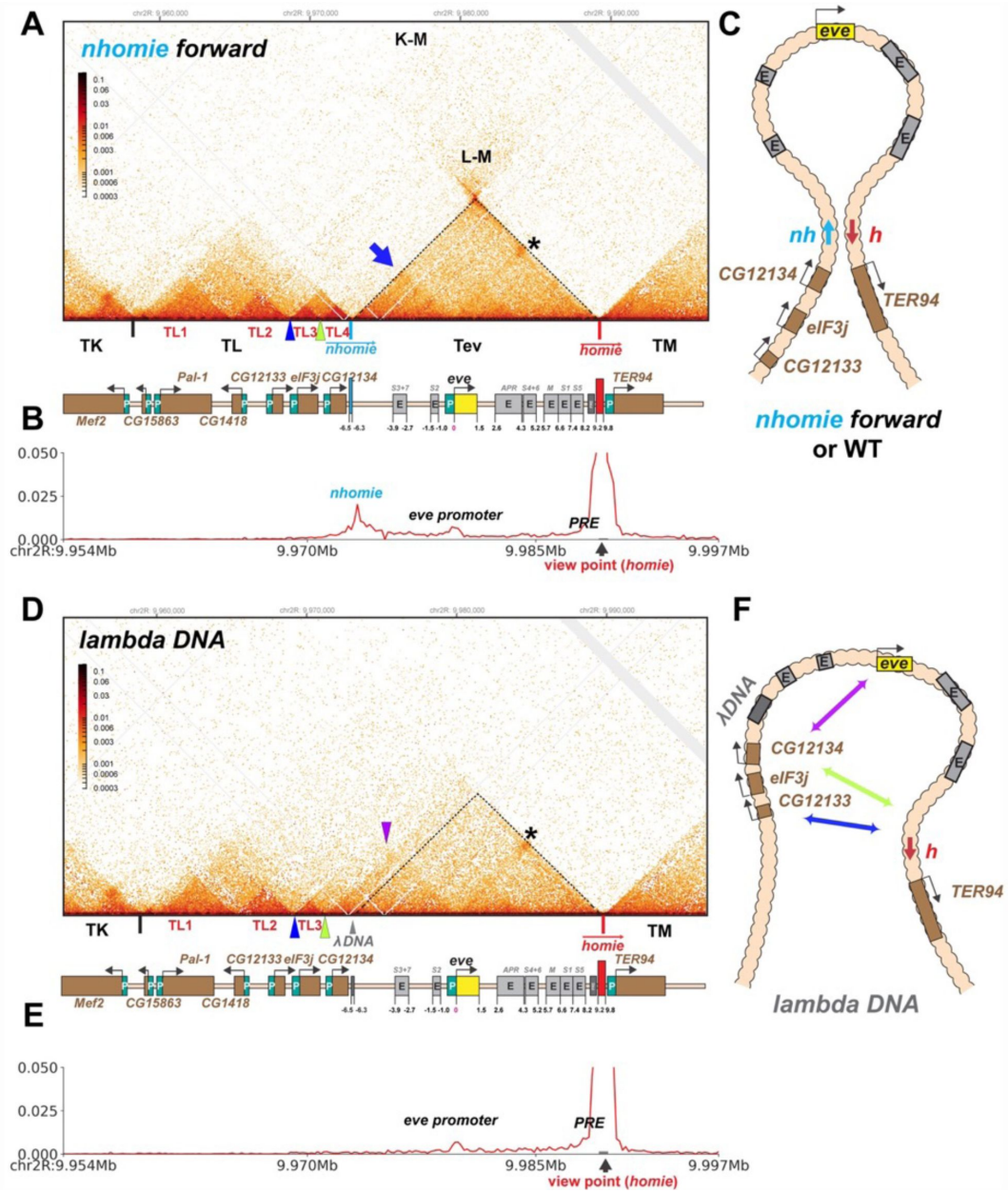

Figure 3.

TAD organization of the *nhomie forward* and *lambda DNA* replacements.

A) MicroC contact profile of 12-16h embryos (stage 12-14) *nhomie forward* embryos. In this, our positive control, *nhomie* replaces endogenous *nhomie*, in the same orientation. N (replicates) = 2. Resolution = 200bp. L-M: Interactions between TADs TL and TM flanking the *eve* locus. Asterisk: sub-TAD linking the *eve* promoter to the *eve* PRE and *homie*. Dark blue arrow: sub-TAD linking the *eve* promoter to *nhomie*. Light blue arrow: *nhomie*. Red arrow: *homie*. Green arrowhead: sub-TAD boundary formed by the *CG12134* promoter region. Dark blue arrowhead: sub-TAD boundary formed by *eIF3j* promoter region. Diagram: Map of *eve* locus and surrounding genes. B) Virtual 4C with viewpoint from *homie* (black arrow) in *nhomie forward* embryos. C) Diagram of the *eve* stem-loop TAD. D) MicroC contact profile of 12-16h *λ DNA* embryos. In this replacement, λ DNA is inserted in place of *nhomie*. N(replicates) = 3. Resolution = 200bp. Asterisk: sub-TAD linking the *eve* promoter to the *eve* PRE and *homie*. Purple arrowhead: sub-TAD linking *CG12134* promoter region to the *eve* promoter. The *eIF3j* sub-TAD TL3 (between the blue and green arrowheads) is still present. E) Virtual 4C with viewpoint from *homie* (black arrow) in *λ DNA* embryos. F) Diagram of the “unanchored” *eve* TAD. Double arrows show novel interactions.

of the *eve* TAD, we did not detect evidence of *eve*-like *TER94* expression (**Figs. 4** and **5**). Thus, the formation and functioning of the TM TAD does not appear to be impacted by the loss of *nhomie* and the fact that left end of the *eve* TAD is no longer properly anchored.

In the case of the gene closest to the *nhomie* deletion, *CG12134*, we were unable to consistently detect transcription driven by the *eve* enhancers in either *nhomie forward* or *λ DNA* embryos. In some *λ DNA* embryos, there were hints of stripes at the blastoderm stage (see **Fig. Supplemental 2**); however, these "stripes" were not observed in most embryos. Since *CG12134* (which forms the TL4 sub-TAD in wild type) is closest to the *eve* enhancers and interacts most strongly, it is possible that the promoter is not compatible with the *eve* enhancers. A different result was obtained for *eIF3j* in *λ DNA* embryos. As shown in the HCR-FISH experiment in **Fig. 4** and quantitated in **Fig. 5**, we observed a series of *eIF3j* stripes over a dark background in pre-cellular blastoderm embryos. As this background hybridization is evident in earlier stages, much of it is likely to be of maternal origin. In contrast to the *λ DNA* replacement, these stripes are not visible in the *nhomie forward* (control) replacement (**Figs. 4** and **5A**). While it is possible to detect all seven stripes in *λ DNA* blastoderm stage embryos, their levels of expression are not equal. The highest levels correspond to *eve* stripes 1, 2, 3 and 7, while *eve* stripes 4, 5 and 6 are expressed at much lower levels. Since the stripe enhancers for 1, 2, 3 and 7 are located between the *eve* promoter and *nhomie*, they are closer to the *eIF3j* promoter than the enhancers for stripes 4, 5 and 6, which are located downstream of the *eve* transcription unit. In addition to possible effects of distance, the subdomain linking the *eve* PRE and *homie* to the promoter is still observed in the *λ DNA* replacement, and this could partially sequester the enhancers located downstream of the *eve* promoter.

We also used digoxigenin *in situ* hybridization to analyze *eIF3j* expression. With this procedure we were able to detect a low level of *eve*-activated *eIF3j* stripe expression in WT and *nhomie forward* embryos at stage 5 (blastoderm) and stages 7-8 (early gastrula: **Fig. Supplemental 3A**). In stage 5 embryos when *eve* expression is driven by specific stripe enhancers, *eIF3j* expression in appears to be similar in all seven stripes (**Fig. Supplemental 3**, WT and *nhomie forward*). In contrast, as was observed in the HCR-FISH experiments (**Fig. 4**), there is a clear bias for enhancers located upstream of *eve* in the *λ DNA* replacement at this point in development. In stage 7-8 embryos, the seven-stripe enhancer drives *eve* expression. It is located close to *nhomie* and, not surprisingly, high levels of *eIF3j* expression are observed in all seven stripes in the *λ DNA* replacement (**Fig. Supplemental 3A**). At later embryonic stages, *eve* expression is driven by tissue-specific neurogenic, mesodermal, and anal plate enhancers. However, *eIF3j* is expressed at high levels in a complex pattern in older embryos, and we were unable to unambiguously detect expression driven by the *eve* enhancers over this background mRNA. This is also not surprising, given that all of the enhancers for these aspects of *eve* expression are located downstream of the *eve* promoter, like the enhancers driving stage 5 stripes 4, 5, and 6.

While the *nhomie* deletion did not have any obvious impact on the level or pattern of *eve* expression in blastoderm stage embryos (see **Fig. 4**), it seemed possible that *eve* activity was not entirely normal. To test this possibility, we mated males homozygous for either *λ DNA* or *nhomie forward* to females heterozygous for a chromosomal deficiency that includes the *eve* gene. We then quantitated the number of missing denticle bands in embryonic cuticle preps. As shown in **Fig. 5B**, the frequency of larvae with "severe" defects (2 or more missing ventral denticle bands) in *nhomie forward* is similar to that in a WT *yw* control. In contrast, in the *λ DNA* replacement, the frequency of larval cuticles with 2 or more missing denticle bands is increased nearly two-fold. Taken together, the increase in severity of the cuticle defects is significant at the $P < 0.01$ level (one-tailed t-test). The A6 denticle belt is missing most frequently, followed by A2, A4, and then A8. These even-numbered abdominal denticle bands are those that are lost in *eve* deficiency mutants (from which the name *even skipped* comes), suggesting that *eve* stripe expression at blastoderm stages is compromised in the embryos that produce these defective cuticles.

Figure 4.

nhomie deletion (*λ DNA* replacement) exposes *eIF3j* to the *eve* enhancers.

nh forward: positive control, as in **Fig. 3**. *λ DNA: nhomie* is replaced with λ DNA. At the syncytial blastoderm stage, a series of stripe-specific enhancers upstream (stripes 1, 2, 3, 7) and downstream (stripes 1, 4, 5, 6) of the *eve* gene drive *eve* expression. During cellularization of the blastoderm and gastrulation, a single enhancer located upstream of *eve* drives expression of all seven stripes. DAPI: DNA stained with DAPI (blue). *eIF3j*: Embryo hybridized with probe complementary to *eIF3j* mRNA. *eve*: Embryo hybridized with probe complementary to *eve* mRNA. *TER94*: Embryo hybridized with probe complementary to *TER94*. Yellow arrowheads: *eve*-enhancer-driven *eIF3j* stripes. Control non-specific probes for each channel indicates autofluorescence background for each channel in the top panel.

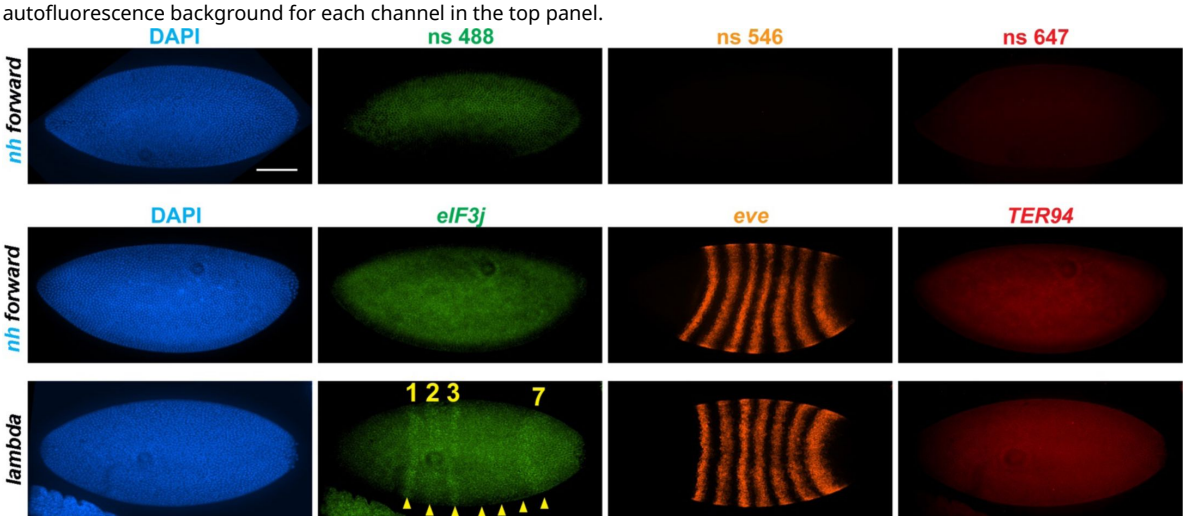

Figure 5.

Manipulating the *nhomie* boundary impacts the regulatory landscape.

N = # of independent replicates, n = # of embryos. Two-way ANOVA with Tukey's multiple comparisons test for each pair of groups was used to determine the statistical significance. *p ≤ 0.05, **p ≤ 0.01, ***p ≤ 0.001 and ****p ≤ 0.0001. A) Quantitation of the number of embryos showing stripe patterns in HCR-FISH for *eIF3j* and *TER94,* as shown in **Figs. 4** and **7**. N = 3. n = 45 for each group. B) Quantitation of the number of missing ventral denticle bands in larvae from a cross of *BSC/CyO,hb-lacZ* deficiency females to males of the indicated genotypes (N = 6): wild-type control (*yw*), n = 767. For the *nhomie forward* replacement, n = 1099; for the *λ DNA* replacement, n = 1175; for the *nhomie reverse* replacement, n = 1083; for the *homie forward* replacement, n = 1137.

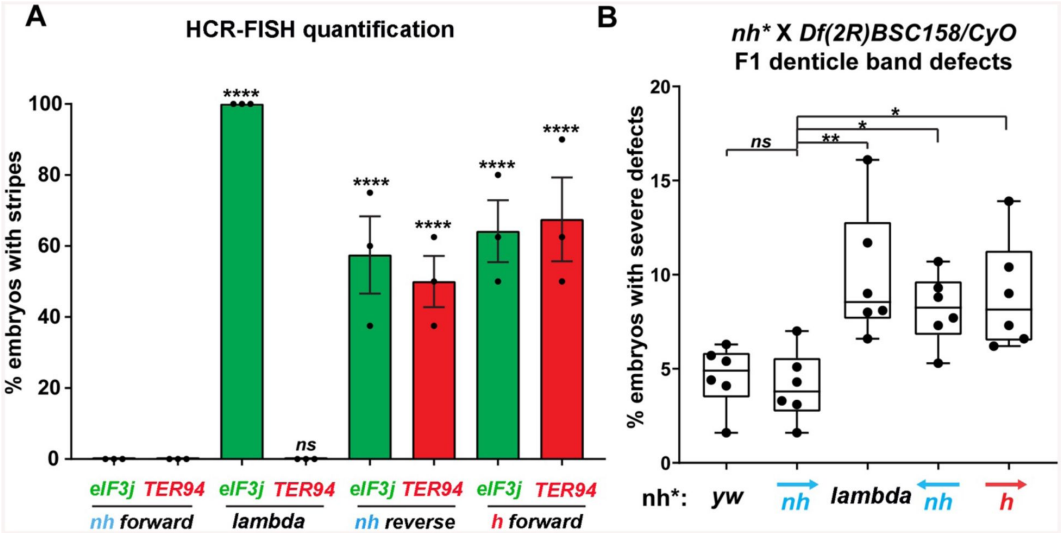

The eve TAD is converted from a stem-loop to a circle-loop by inverting nhomie

The orientation of boundary:boundary pairing interactions determines the topology of each chromatin loop (Bing et al. 2024; Fujioka et al. 2016). Since *nhomie* and *homie* pair with each other head-to-tail, the endogenous *eve* TAD is a stem-loop. This orientation dependence means that one can convert the *eve* TAD from a stem-loop to a circle-loop by inverting the *nhomie* boundary. If our expectations are correct, the MicroC contact pattern will also be transformed from a volcano triangle with a plume to one in which sequences in the *eve* TAD is flanked by a cloud of crosslinked sequences from both neighboring TADs (TL and TM), like that observed in the *Abd-B* region of BX-C.

We tested this prediction by inserting the *nhomie* boundary in the reverse orientation (*nhomie reverse*). **Fig. 6A** shows that the *eve* TAD is reconstituted by *nhomie reverse* (compare with **Fig. 3**). The sub-TAD evident in the *nhomie forward* replacement linking *nhomie* to the *eve* promoter is also re-established (blue arrow). In addition, consistent with our expectation, the plume topping the *eve* TAD is gone and is replaced by a much more sparsely populated LDC domain (purple double-arrow and above). The more prominent LDC TAD-TAD interactions (the clouds) are between sequences in the *eve* TAD and the neighboring TADs. On the right, *eve* forms an LDC interaction domain with TM (ev-M). On the left, *eve* interacts most strongly with sequences in TL4, and progressively less strongly with sequences in the sub-TADs TL3, TL2, and then TL1 (L-ev). In addition to restoring the *eve* TAD, the TL TAD is re-established, indicating that the *nhomie* boundary is important in defining both endpoints of the TL TAD. On the other hand, with the exception of the *CG12133* sub-TAD, *nhomie* does not play a role in generating the three other sub-TADs in the TL TAD. The other interesting feature is a 45° band of interaction (just below the purple double-arrow) that includes interactions between sequences in TL4 and sequences in *eve* that appear to be located near the left edge of *homie*. These sequences likely correspond to the *eve* 3' PRE (Fujioka et al. 2008), located just inside the 3' end of the *eve* TAD.

Insulation is reduced in nhomie reverse

Consistent with the models for stem-loops and circle-loops in **Fig. 1**, the neighborly interactions evident in the MicroC contact patterns for *nhomie forward* and *nhomie reverse* are quite distinct. The *nhomie forward* TAD is isolated from its neighbors, and crosslinking between *eve* and the neighboring TADs is suppressed (**Figs. 1B** and **2A**). This is not true for the circle-loop TAD generated by *nhomie reverse*: in this configuration, the *eve* TAD is not sequestered from neighboring TADs (**Figs. 1D** and **2B**), but instead interacts much more frequently with sequences in next-door TADs than in the stem-loop configuration. Since the *eve* TAD is no longer as well-isolated from its neighbors, this could increase the frequency of "productive" interactions between *eve* regulatory elements and genes in nearby TADs, and vice versa.

To test whether the circle-loop topology has an impact on the regulatory landscape, we hybridized *nhomie reverse* embryos with HCR-FISH probes for *eIF3j*, *TER94* and *eve*. In early blastoderm stage *nhomie forward* embryos, there is little evidence of *eIF3j* or *TER94* expression driven by *eve* stripe enhancers, and the HCR-FISH hybridization pattern is uniform (see **Fig. 4**). In contrast, it is possible to discern individual stripes of both *eiF3j* and *TER94* mRNA over the background signal in a subset of *nhomie reverse* blastoderm stage embryos in HCR-FISH (**Fig. 7**). Since these genes are assembled into their own topologically independent looped domains rather than being in the same domain as *eve*, the level of *eiF3j* and also *TER94* stripe expression is lower than that observed in the *nhomie* deletion (*λ DNA*). The *nhomie reverse* circle-loop also differs from the *nhomie* deletion (*λ DNA*) in that there is not such an obvious preference for which *eve* enhancers activate expression. In addition, *eve*-dependent *eiF3J* and *TER94* stripes are detected in only about half of the blastoderm stage embryos (**Fig. 5A**). It is possible that the frequency of productive inter-TAD

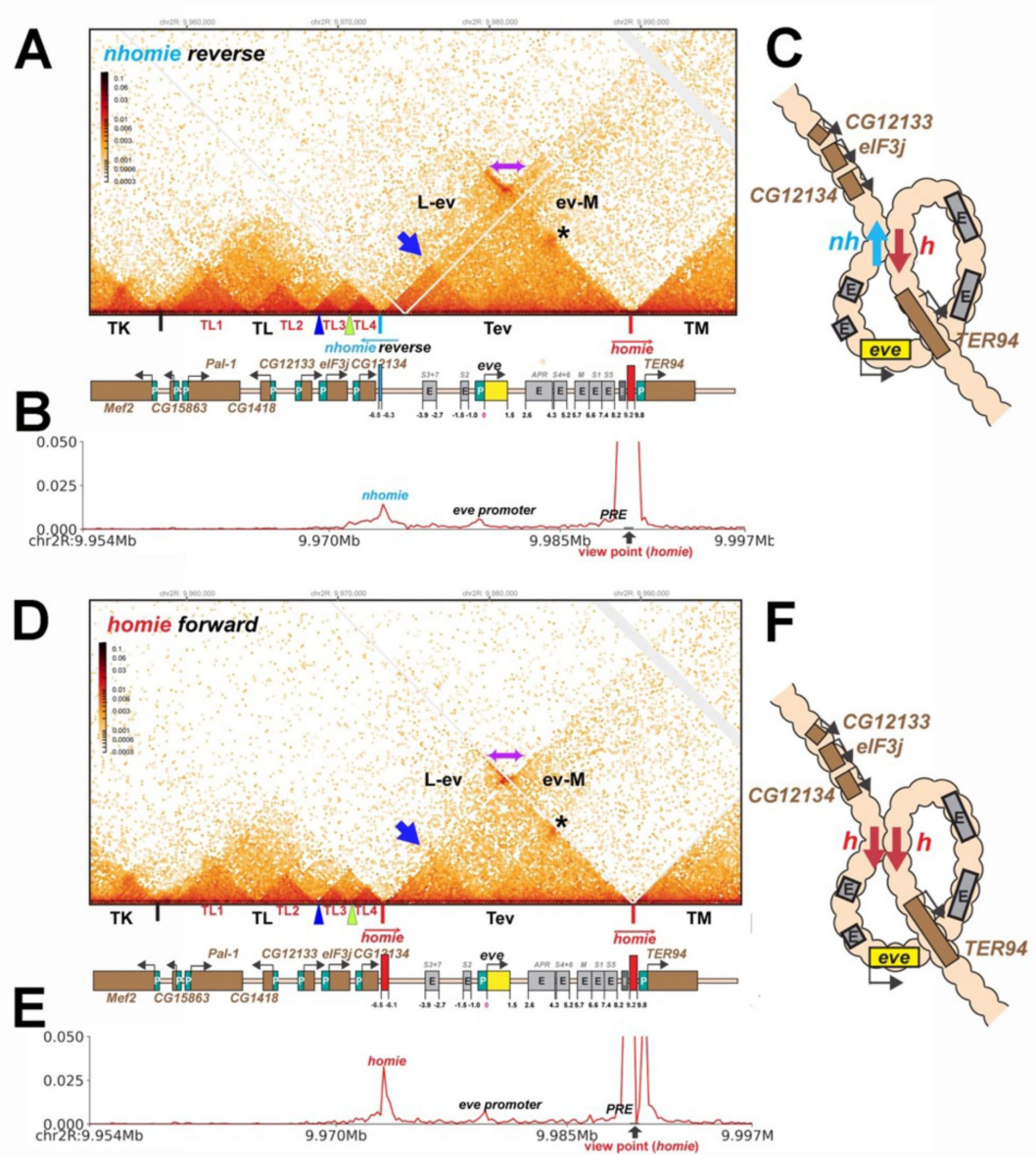

Figure 6.

TAD organization of the *nhomie reverse* and *homie forward* replacements.

A) MicroC contact profile of 12-16h *nhomie reverse* embryos. In this replacement, *nhomie* is inserted in the reverse orientation compared to WT *nhomie*. N (replicates) = 3. Resolution = 200bp. B) Virtual 4C with viewpoint from *homie* (black arrow) in *nhomie reverse* embryos. C) Diagram of the *nhomie reverse:homie* circle-loop. D) MicroC contact profile of 12-16h *homie forward* embryos. In this replacement, *homie* is inserted in the forward orientation (the same as the endogenous *homie*): N (replicates) = 3, resolution = 200bp. E) Virtual 4C with viewpoint from *homie* (black arrow) in *homie forward* embryos. F) Diagram of the *homie forward:homie* circle-loop. A) and C): Note that interactions between the TADs flanking the *eve* locus (purple double arrow) are suppressed compared to *nhomie forward* (see **Fig. 3**), while interactions of the *eve* TAD (Tev) with TL and TM are enhanced (L-ev and ev-M). Asterisk: sub-TAD linking the *eve* promoter to the *eve* PRE and *homie*. Dark blue arrow: sub-TAD linking the *eve* promoter to *nhomie reverse*. Light blue arrow: *nhomie reverse*. Red arrow: *homie*. Green arrowhead: sub-TAD boundary formed by the *CG12134* promoter region. Dark blue arrowhead: sub-TAD boundary formed by the *eIF3j* promoter region.

contacts differs from one embryo to the next; however, a more likely reason is that the high background of *eIF3j* and *TER94* transcripts obscures the low level of *eve* enhancer-driven expression at this stage. Once the seven-stripe enhancer is activated, *eve*-dependent *TER94* expression in *nhomie reverse* is elevated, and all seven stripes are observed (**Fig. Supplemental 3B**). This fits with the MicroC contact profile. As shown in **Fig. 6A**, the *TER94* gene is preferentially crosslinked to *eve* sequences located between *nhomie reverse* and the *eve* promoter as compared to sequences spanning the *eve* gene and the downstream enhancers (i.e., the upper left portion of the ev-M region shows more crosslinking than does the lower right portion). This bias correlates with the location of the 7-stripe enhancer, located near the 5' end of the *eve* TAD. By contrast, there is much less seven-stripe enhancer-driven expression of *eIF3j* (**Fig. Supplemental 3A**) than of *TER94*. Consistent with this observation, crosslinking between *eIF3j* and sequences in *eve* close to *nhomie reverse* and the seven-stripe enhancer occur less frequently than crosslinking to sequences on the other side of the *eve* TAD (i.e., the lower left portion of the L-ev region of the MicroC profile shows less crosslinking than does the upper right portion), although this crosslinking bias may not be as pronounced as that observed between *TER94* and the two sides of the *eve* TAD.

While *eve* stripe expression is not discernably different from wild type, the circle-loop topology still impacts *eve* function. As shown in **Fig. 5B**, the fraction of *nhomie reverse* embryos with 2 or more missing denticle bands is nearly twice that in either *yw* or the *nhomie forward* replacement. Taken together, the increase in severity of the cuticle defects is significant at the $P < 0.05$ level (one-tailed t-test). As was observed for the *λ DNA* replacement, the A6 denticle band is missing most frequently, followed by A2, A4 and then A8.

homie forward converts the eve stem-loop to a circle-loop

While the findings in the previous section show that loop topology impacts how sequences in TADs interact with each other and with their neighbors, one might argue that the effects we observed are a reflection of some novel properties of the *nhomie* boundary when it is inverted. To test this possibility, we took advantage of the fact that in addition to pairing with *nhomie*, the *homie* boundary pairs with itself (Fujioka et al. 2016). However, unlike *nhomie:homie* pairing, which is head-to-tail, *homie:homie* pairing is head-to-head. This means that it is possible to convert the *eve* TAD into a circle-loop by inserting *homie* into the *nhomie* deletion in the forward orientation.

As shown in **Fig. 6D**, the MicroC contact profile of *homie forward* is similar to that observed for *nhomie reverse*. The plume topping the *eve* TAD in wild type (**Fig. 2A**) or in *nhomie forward* (**Fig. 3A**) is absent. Likewise, instead of being isolated from its neighbors, the *eve* TAD contacts TL and TM. Also like *nhomie reverse*, *homie forward* forms a subdomain within the *eve* TAD linking it to sequences in the *eve* promoter. There is also enhanced crosslinking between sequences in TL4 and sequences on the right end of the *eve* TAD that correspond to the *eve* 3' PRE (Fujioka et al. 2016).

The MicroC pattern is not the only similarity between *homie forward* and *nhomie reverse*. The functional properties of the *homie forward eve* TAD are also similar. **Fig. 7** shows that the *eve* enhancers weakly activate both *eIF3j* and *TER94*. As was the case for *nhomie reverse*, expression levels at the blastoderm stage are low and are observed in only about half of the embryos (**Fig. 5A**). After the blastoderm stage, when the seven-stripe enhancer drives *eve* expression, an even higher level of *TER94* expression is observed (**Fig. Supplemental 3B**). In addition, the functioning of the *eve* gene when it is in the circle-loop configuration is not as efficient, and the frequency of *homie forward* embryos with 2 or more missing denticle bands is twice that of *nhomie forward* (**Fig. 5B**). Taken together, the increase in severity of the cuticle defects is significant at the $P < 0.05$ level (one-tailed t-test).

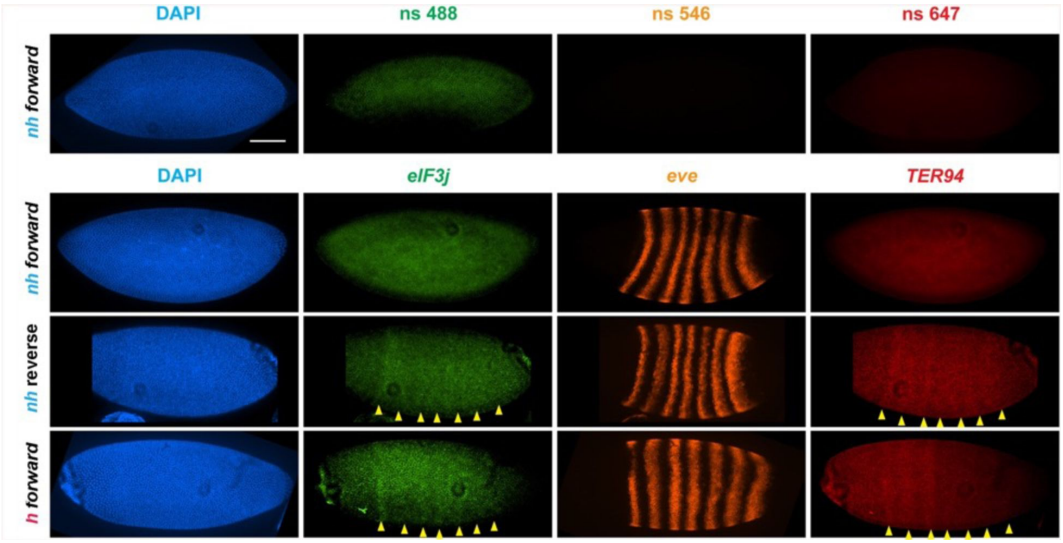

Figure 7.

eve enhancers activate neighboring genes when the *eve* TAD is a circle-loop.

HCR-FISH hybridization to mRNA expressed by *eIF3j*, *eve* and *TER94* at the blastoderm stage (embryonic stage 5). *nh forward*: *nhomie* is replaced with *nhomie* in the forward (normal) orientation (positive control, as in **Fig. 3**). *nh reverse*: *nhomie* is replaced with *nhomie* in the reverse orientation. *h forward: nhomie* is replaced with *homie* in the forward orientation. Yellow arrowheads: positions of stripes. DAPI (blue): DNA stained with DAPI. *eIF3j* (green): embryo is hybridized with probe complementary to *eIF3j* mRNA. *eve* (orange): embryo is hybridized with probe complementary to *eve* mRNA. *TER94* (red): embryo is hybridized with probe complementary to *TER94*. Control non-specific probes for each channel indicates autofluorescence background for each channel in the top panel.

Discussion

Two different though overlapping classes of chromosomal architectural elements have been identified in flies. One class is the PREs found in many developmental loci. PREs were first discovered because they induce pairing-sensitive silencing of reporter genes (Americo et al. 2002; Kassis et al. 1991). More recent studies have shown that the ability of these elements to physically pair with each other may be their most important function (Batut et al. 2022; Levo et al. 2022). The other class of architectural elements are chromatin boundaries (also called insulators). PRE pairing in *cis* typically takes place within the context of a larger chromosomal domain, or TAD. In contrast, boundary elements are responsible for defining the endpoints of these looped domains (Arzate-Mejía et al. 2020; Batut et al. 2022; Bing et al. 2024; Chetverina et al. 2017; Ibragimov et al. 2023; Stadler et al. 2017). While not much is known about the parameters governing PRE pairing, the pairing interactions of fly boundaries have been studied in some detail. The key features include an ability to engage in promiscuous pairing interactions, distinct partner preferences, and orientation dependence. Of the endogenous (non-*gypsy*) boundaries whose functional properties have been studied in detail, only one, *Fab-7*, appears to be able to pair in both orientations. However, *Fab-7* may be unusual in that its boundary activity depends upon factors that have been implicated in the functioning of PREs (Kyrchanova et al. 2018). For all of the other boundaries studied so far, pairing interactions are orientation-dependent. When fly boundaries pair with themselves, the interactions are head-to-head (Kyrchanova et al. 2008a). This make sense, as the available evidence suggests that self-pairing interactions in *trans* may be largely responsible for the pairing of homologous chromosomes in precise register (Erokhin et al. 2021; Fujioka et al. 2016). In this case, head-to-tail self-pairing would uncouple the loops on the two homologs (and sister chromatids).

Unlike self-pairing in *trans*, pairing interactions between heterologous boundaries in *cis* can be head-to-head or head-to-tail. The topological consequences are quite distinct. The former generates a circle-loop, while the later forms a stem-loop (Chetverina et al. 2017). In the studies reported here, we have investigated how these two different topologies impact the local chromatin organization. We have also determined whether circle-loops and stem-loops alter the ability of boundary elements to define units of independent gene activity and insulate against regulatory interactions between neighboring TADs.

nhomie deletion disrupts the eve TAD

As would be predicted from many different studies (c.f., (Cavalheiro et al. 2021; Chetverina et al. 2017), deletion of the *nhomie* boundary and replacement with a control *λ DNA* disrupts the *eve* TAD and alters the regulatory landscape. The MicroC profile shows that disruption of the *eve* TAD and the neighboring TADs is one-sided. Within the *eve* TAD, the subdomain linking *homie* and the nearby PRE to the *eve* promoter is unaffected. Likewise, the large TAD, TM, which encompassess both *TER94* and *pka-R2*, and is defined at one end by *homie* and at the other by an uncharacterized boundary element upstream of the *pka-R2* promoter, is intact (**Fig. Supplemental 1B**). In contrast, on the *nhomie* side of the *eve* TAD, the sub-TAD linking *nhomie* to the *eve* promoter is absent, and is replaced by a less well-defined sub-TAD linking the *eve* promoter to an element near the *CG12134* promoter. However, the end-point of the *eve* TAD is no longer distinct, and *eve* sequences are now crosslinked to the *eIF3j* sub-TAD and to sequences in the more distant TL sub-TADs TL3, TL2 and TL1. Consistent with these alterations in the physical organization of the *eve* and neighboring TADs, the *TER94* gene is still insulated from the *eve* enhancers. While sequences in the *eve* TAD physically interact with the gene closest to *nhomie*, *CG12134*, only the next gene over, *eIF3j*, is clearly activated by the *eve* enhancers. Since crosslinking between sequences in *CG12134* and the *eve* TAD is more frequent than crosslinking between the *eIF3j* sub-TAD TL3 and the *eve* TAD, it seems likely that *CG12134* is refractory to activation by the *eve* enhancers. This

could be due to an incompatiblity between the *CG12134* promoter and the *eve* enhancers. Alternatively, the promoter may not be active at this stage. While *eIF3j* is activated by the *eve* enhancers in stage 5 embryos in the *nhomie* deletion, the stripe enhancers located upstream of the *eve* gene drive a higher level of expression than those located downstream. Two factors in addition to the effects of distance could potentially account for this finding. Since the *eve* promoter is located between the downstream enhancers and the *eIF3j* gene, activation of *eIF3j* by the downstream enhancers could be suppressed by promoter competition. Alternatively, or in addition, the sub-TAD formed between the 3' PRE/*homie* and the *eve* promoter/proximal PRE (Fujioka et al. 2008) could tend to isolate the downstream *eve* stripe enhancers from interactions with *eIF3j*.

Topology impacts local 3D genome organization and the potential for regulatory interactions

In boundary bypass experiments using endogenous fly boundaries, the ability of the upstream enhancers to activate the downstream reporter depended on the topology of the loop generated by the paired boundaries (Kyrchanova et al. 2008a). Activation is observed for stem-loops, as this configuration brings the upstream enhancers into close proximity with the downstream reporter. In contrast, the enhancers and downstream reporter are not brought into contact when the topology is a circle-loop. As would be predicted from these bypass experiments, the stem-loop formed by the head-to-tail pairing of *nhomie* and *homie* physically isolates the *eve* TAD from its neighbors, and this is reflected in the low density of contacts between sequences in *eve* and the neighboring TADs (**Fig. 2A**). Conversely, the TADs that flank *eve* are brought together, and contacts between them generate the plume that is observed above the *eve* volcano triangle.

The physical isolation afforded by the stem-loop topology is lost when the *eve* TAD is converted to a circle-loop, either by inverting the *nhomie* boundary or by replacing *nhomie* with the *homie* boundary inserted in the forward direction (**Fig. 6**). In the former case, head-to-tail *nhomie*:*homie* pairing generates a circle-loop. In the latter case, head-to-head pairing of *homie* (inserted in the forward orientation) with endogenous *homie* generates a circle-loop. The alteration in the local 3D organization induced by the conversion of *eve* to a circle-loop is evident from the changes in the MicroC contact pattern. Instead of being isolated from neighboring TADs, the *eve* TAD interacts not only with its immediate neighbors, but also with more distant TADs. As a result, the plume of enhanced contacts linking TM to TL, TK, and TJ is absent and is replaced by contacts between these TADs and the *eve* TAD.

As might be expected from the MicroC contact patterns, the conversion to a circle-loop topology is accompanied by alterations in regulatory interactions between *eve* and the genes in the neighboring TADs (**Fig. 7** and **Fig. Supplemental 3**). Unlike the *nhomie forward* replacement, the *eve* stripe enhancers in both of the circle-loop replacements are able to weakly activate expression of two neighboring genes, *eIF3j* and *TER94*. This pattern of activation mirrors the enhancement in contacts between the *eve* TAD and the neighboring TL and TM TADs evident in MicroC experiments. Thus, though *eIF3j* and *TER94* are clearly shielded from the *eve* enhancers when the *eve* TAD is a circle-loop, a greater degree of isolation from the action of the *eve* enhancers is afforded when the *eve* TAD is a stem-loop.

In addition to reducing insulation from regulatory interactions with genes in neighboring TADs, the circle-loop topology impacts the functioning of the *eve* gene (**Fig. 5B**). For both *nhomie reverse* and *homie forward*, the frequency of multiple denticle band defects compared to the *nhomie forward* control is enhanced in a sensitized genetic background. While we did not detect any obvious reductions in the *eve* stripes in blastoderm stage embryos, the circle-loop provides less insulation than the stem-loop, and it is possible that the neighboring promoters suppress *eve* expression by competing for the *eve* enhancers. Another (non-mutually exclusive) possibility comes from the studies of Yokoshi et al. (Yokoshi et al. 2020), who used live imaging to examine

the effects of flanking a reporter with the *nhomie* and *homie* boundaries. In their experiments, reporter expression was enhanced over two-fold when the reporter was flanked by *nhomie* and *homie*; however, the enhancement was greater when the paired boundaries formed a stem-loop than when they formed a circle-loop.

Boundary:boundary pairing can generate stem-loops and circle-loops

Our manipulations of the *nhomie* boundary support the notion that TADs can have two different loop topologies, stem-loop and circle-loop, and these topologies impact their physcial and biochemical properties. Since circle-loop TADs cannot be generated in the popular cohesin loop extrusion/CTCF roadblock model for the sculpting the 3D genome, it would be important to know whether there are other unambiguous examples of loops with either a stem-loop or circle-loop topology besides those described here. As discussed above, the available evidence suggests that the boundaries in the *Abd-B* regulatory domains pair with their neighbors head-to-head, and thus form circle-loops. While the contact pattern between neighbors in the *Abd-B* region fit with that expected for an array of circle-loop TADs, this has not been confirmed by examining the MicroC profiles before and after manipulating the boundary elements in this region. For this reason we sought unambiguous examples of chromatin loops generated by the orientation-dependent pairing of endogenous TAD boundaries that have either a stem-loop or a circle-loop topology. The collection of meta-loops described recently by Mohana et al. (2023) provide one such test, as many appear to be generated by the pairing of TAD boundaries, and their local interaction profiles are easily interpreted.

Shown in **Fig. 8A** is a 2.8 Mb meta-loop on chromosome 2L generated by the pairing of two TAD boundaries, labeled blue and purple (block arrows). The pairing of the blue and purple TAD boundaries brings sequences in the TADs flanking the two boundaries into contact, and this generates two rectangular boxes of interaction indicated by the arrows (see also blue double arrows in the diagram on the right). In the rectangular box on the upper left of the contact map, sequences in the TAD containing *CG33543*, *Obp22a* and *Npc2a* located just upstream of the blue boundary are crosslinked to sequences upstream of the purple boundary in the TAD containing the *fipi* gene. In the rectangular box on the lower right, sequences in a small TAD downstream of the blue boundary (which contains *Nplp4* and *CG15353*) are crosslinked to sequences in a TAD downstream of the purple boundary (which contains *CG3294* and *slf*). As shown in the diagram, this pattern of interaction (upstream-to-upstream and downstream-to-downstream) indicates that the blue and purple TAD boundaries pair with each other head-to-head, and this orientation generates a large loop with a circle-loop topology.

The 2.2 Mb meta-loop on chromosome 3L in **Fig. 8B** is more complicated in that it is generated by four TAD boundaries (indicated by blue, brown, green and purple arrows). The blue and brown boundaries separate a small TAD containing *CG7509* from two larger TADs, while the green and blue boundaries define the endponts of a TAD containing the most distal promoter (blue arrowhead) of the *Mp* (*Multiplexin*) gene. As indicated in the accompanying diagram, the brown and green boundaries pair with each other head-to-tail as do the blue and purple boundaries. Pairing of the brown and green boundaries generates a large ~2.2 Mb stem-loop that brings sequences in the TAD downstream of the brown boundary, which contains the *Dhc64C* and *CG1808* genes, into contact with sequences in the TAD upstream of the green boundary, which contains the *CG3238* and *bin* (*binou*) genes. This linkage generates the rectangular box of enhanced contacts in the lower left corner of the contact map. Pairing of the blue and purple boundaries generates a small stem-loop bubble that links sequences in the *CG7509* TAD to the TAD containing the *Mp* distal promoter (blue arrowhead). This connection generates a small rectangular box of enhanced crosslinking in the center of the contact map. In addition, sequences upstream of the blue boundary and downstream of the purple boundary are brought into contact by the head-to-tail pairing of these two boundaries. This generates a third rectangular box of enhanced physical

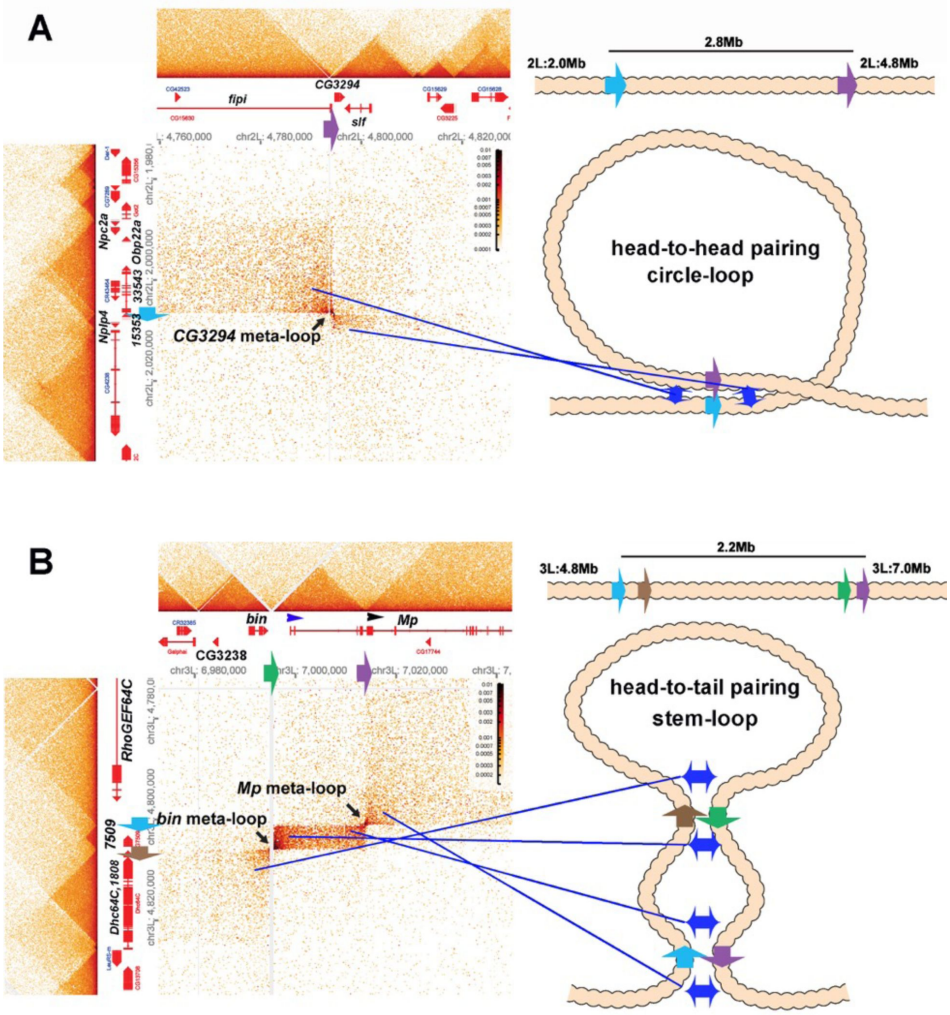

Figure 8.

Circle-loop and stem-loop meta-loops.

A) *CG3294* circle-loop meta-loop. In this meta-loop, a TAD boundary (blue arrow) located at ~2.0 Mb on chromosome 2L pairs head-to-head with a TAD boundary (purple arrow) located ~2.8 Mb away. As indicated in the diagram, head-to-head pairing generates a circle-loop. In the circle-loop topology, the TAD upstream of the blue boundary is brought into contact with the TAD upstream of the purple boundary, as indicated the diagram (blue double arrows). This generates a rectangular box of enhanced contacts between sequences in the TAD containing the *CG33543*, *Obp22a* and *Npc2a* genes and sequences in a TAD that contains the *fipi* gene. This box is located on the upper left of the contact map (above and to the left of the black arrow). Sequences in TADs downstream of the blue and purple boundaries are also linked, and this generates a small rectangular box representing sequences in the small *Nplp4* and *CG15353* TAD ligated to sequences in the TAD containing *CG3294* and *slf* (below and to the right of the black arrow). B) The *bin/Mp* meta-loops on the left arm of the 3rd chromosome are generated by the head-to-tail pairing of two sets of boundaries, indicated by the blue, brown, green and purple arrows. Pairing of the brown and green boundaries generates a ~2.2 Mb stem-loop. Sequences in the TAD downstream of the brown boundary (which contains the *Dhc64C* and *CG1808* genes) are linked to sequences in the TAD upstream of the green boundary (which contains *CG2328* and *bin*). This generates the rectangular box of enhanced contacts on the lower left of the contact map. Pairing of the blue and purple boundaries head-to-tail generates a small stem-loop “bubble” (see diagram). This bubble brings sequences in the TAD containing the most distal *Mp* promoter (blue arrowhead) into contact with sequences in the small TAD containing *CG7509* (see diagram on the right). Interactions between these two TADs generates the small rectangular box of enhanced contacts in the center of the contact map. The head-to-tail pairing of the blue and purple boundaries also bring sequences in the TAD upstream of the blue boundary that contains the *RhoGEF64C* gene into contact with the TAD containing one of the internal *Mp* promoters (black arrowhead). This interaction generates the box of enhanced contacts in the upper right portion of the contact map. The bin size for each panel is 200 bp; embryos are 12-16h old.

contact in the upper right corner of the contact map which links sequences in the TAD containing the *RhoGEF64C* gene to sequences in the TAD containing the internal *Mp* promoter (black arrowhead). Note that the positioning of the lower left and upper right retangular boxes of enhanced contact in the *bin-MP* meta-loop is the mirror image of the rectangular boxes of enhanced contact for the *CG3294* meta-loop.

Stem-loops versus circle-loops

The results we have reported here demonstrate that boundary:boundary pairing in flies generates loops that can have either a stem-loop or a circle-loop topology. An important question is what is the relative frequency of stem-loops versus circle-loops in the fly genome? The MicroC contact patterns for the stem-loop and circle-loop versions of the *eve* TAD are quite distinct. The former is a volcano triangle with a plume while the latter is a volcano triangle flanked by clouds. A survey of the MicroC contact patterns elsewhere in the non-repetitive regions of the fly genome indicates that volcanoes with plumes are rare (~30). For example, there are two volcano triangles with plumes in the *Antennapedia* complex, and they encompass the *deformed* and *fushi-tarazu* genes (Levo et al. 2022). However, since most of the "euchromatic" regions of the fly genome are assembled into TADs whose MicroC profiles resemble that observed for *eve* circle-loops and the *Abd-B* region of BX-C, it is possible that much of the fly genome is assembled into circle-loops, not stem-loops.

While this suggestion is consistent with the available data, it is based on contact patterns between neighboring TADs, and important caveats remain. For one, the contact patterns between neighboring TADs can deviate in one way or another from that seen in the *Abd-B* region. For example, there are TADs in which interactions with one set of neighbors appears to be suppressed as expected for stem-loops, but the classic plume is absent, as interactions are not suppressed with the other neighbors (c.f., **Fig. Supplemental 4A**). In other cases, there are a series of complicated TAD-TAD interactions topped by a rectangular plume (**Fig. Supplemental 4B**: purple arrow). For this reason, it will not be possible to draw firm conclusions about the frequency of stem-loops versus circle-loops genome-wide until the relative orientation of the paired boundaries themselves can be determined directly. On the other hand, it is clear from our studies that both classes of TADs must exist in flies. If, as seems likely, a significant fraction of the TADs genome-wide are circle-loops, this would effectively exclude cohesin-based loop extrusion as a general mechanism for TAD formation in flies. In addition, though stem-loops could be generated by a cohesin-dependent mechanism, it is unlikely that this mechanism is operational in flies, as we have shown here and in Bing, et al. (Bing et al. 2024) that stem-loops in flies are formed by orientation-dependent boundary:boundary pairing.

Another important question is whether our findings have any relevance to the formation and topology of TADs in mammals. In the most common version of the loop extrusion model, the mammalian genome is assembled into an alternating pattern of stem-loops and unanchored loops (c.f., (Davidson and Peters 2021; Higashi and Uhlmann 2022; Perea-Resa et al. 2021). In this case, one might expect to observe volcano triangles topped by plumes alternating with DNA segments that have a considerably lower densisty of internal contacts. However, this crosslinking pattern is not observed in published MicroC data sets (Hsieh et al. 2020; Krietenstein et al. 2020). Instead of an alternating pattern of high-density TAD triangles separated by regions of low density contacts, the TAD triangles are generally linked to both neighbors, just as in flies. Moreover, also like in Drosophila, there are few stem-loop volcano TADs topped by plumes. Instead, the crosslinking pattern between neighboring TADs appears similar to that observed for circle-loops in flies. Of course, one problem with these MicroC studies is that the resolution may not be sufficient to detect volcanos with plumes or the other features predicted by the loop extrusion model. However, there are no obvious volcanoes with plumes in the much higher resolution RCMC studies of Goel et al. (Goel et al. 2023). Instead, the MicroC profiles most closely resemble those seen in the *Abd-B* region of BX-C (c.f. the *Ppm1g* locus in **Fig. 4** of (Goel et al. 2023). Moreover, compromising cohesin activity has minimal impact on the TADs in this region

of the mouse genome, as evidenced from the MicroC pattern before and after knockdown. Based on these observations, one can reasonably question whether cohesin-mediated loop extrusion is deployed in mammals as the mechanism for not only generating TADs but also determining TAD boundaries. Clearly validation of the loop extrusion/CTCF road-block model as currently formulated will require a direct demonstration that mammalian TADs are exclusively either stem-loops or unanchored loops, and that the endpoints are always (or almost always) determined by CTCF roadblocks.

Acknowledgements

We would like to thank Gordon Grey for running the fly food facility at Princeton, members of the Lewis Sigler Genomics Core facility for their invaluable assistance with DNA sequencing, and Qing Liu for excellent technical assistance. We would also like to thank members of MOL431 for creative input. Special thanks to Olga Kyrchanova, Daria Chetverina, Maksim Erokhin, Pavel Georigev, Tsutomu Aoki, Girish Deshpande, Airat Ibragimov, Sergey Ryabichko, Yuri Pritykin, Alex Ostrin, Xinyang Bing, Xiao Li and Mike Levine for stimulating discussions and sharing unpublished data.

Materials and methods

Key resources table

REAGENT or RESOURCE	SOURCE	IDENTIFIER
Chemicals, peptides, and recombinant proteins		
n-Heptane	Fisher Chemical	O3008-4
Paraformaldehyde 20% solution, EM Grade	Electron Microscopy Sciences	15713-S
Formaldehyde, 16%, methanol free, Ultra Pure	Polysciences Inc	18814-10
PBS - Phosphate-Buffered Saline (10X) pH 7.4, RNase-free	Thermo Fisher	AM9624
Tween 20	Sigma	P1379
Triton X-100	Bio-Rad	161-0407
Tris base	Sigma	11814273001
Methanol	Fisher Chemical	203403
SSC, 20X	Thermo Fisher	15557044
Formamide	Thermo Fisher	17899
Dextran sulfate	Sigma	D8906
Salmon Sperm DNA	Thermo Fisher	AM9680
Ribonucleoside Vanadyl Complex	NEB	S1402S
Nuclease-free BSA	Sigma	126609
Triethylammonium Acetate	Sigma	625718
dGTP (100 MM)	VWR	76510-208
dTTP (100 MM)	VWR	76510-224
Lonza NuSieve 3:1 Agarose	Thermo Fisher	BMA50090
T4 DNA ligase	NEB	M0202L
Biotin-11-dCTP	Jena Bioscience	NU-809-BIOX
Biotin-14-dATP	Jena Bioscience	NU-835-BIO14

Qubit dsDNA HS Assay Kit	Life Technologies Corp.	Q32851
Atto 633 NHS ester	Sigma	01464
Phase Lock Gel™, QuantaBio - 2302830, Phase Lock Gel Heavy	VMR	10847-802
NEBNext Ultra II DNA Library Prep Kit for Illumina	NEB	E7645S
Ampure Xp 5ml Kit	Thermo Fisher	NC9959336
Hifi Hotstart Ready Mix	Thermo Fisher	501965217
Dynabeads MyOne Streptavidin C1	Life Technologies Corp.	65001
cOmplete™, EDTA-free Protease Inhibitor Cocktail	Sigma	11873580001
N,N-Dimethylformamide	Sigma	227056
Potassium acetate solution	Sigma	95843
DSG (disuccinimidyl glutarate)	Thermo Fisher	PI20593
T4 Polynucleotide Kinase - 500 units	NEB	M0201S
DNA Polymerase I, Large (Klenow) Fragment - 1000 units	NEB	M0210L
End-it DNA End Repair Kit	Thermo Fisher	NC0105678
Proteinase K recomb. 100 mg	Sigma	3115879001
Nuclease MicroCoccal (s7)	Thermo Fisher	NC9391488
EGS (ethylene glycol bis(succinimidyl succinate))	Thermo Fisher	PI21565
Atto 565 NHS ester	Sigma	72464
HCR™ RNA-FISH Custom Probe Set: eve	Molecular Instruments	
HCR™ RNA-FISH Custom Probe Set: ter94	Molecular Instruments	
HCR™ RNA-FISH Custom Probe Set: CG12134	Molecular Instruments	
HCR™ RNA-FISH Custom Probe Set: eIF3j	Molecular Instruments	
HCR™ Amplifier B1, 488	Molecular Instruments	
HCR™ Amplifier B2, 564	Molecular Instruments	

HCR™ Amplifier B3, 647	Molecular Instruments	
HCR™ Buffers	Molecular Instruments	
NEBNext Multiplex Oligos for Illumina	NEB	E7335S
Software and algorithms		
Fiji (ImageJ)	Schindelin et al. (Schindelin et al. 2012)	fiji.sc
NIS element	Nikon	microscope.healthcare.nikon.com/products/software/nis-elements
Graphpad Prism 8	GraphPad Software	graphpad.com
HiGlass	Kerpedjiev et al. (Kerpedjiev et al. 2018)	higlass.io
bwa	Li H. and Durbin R. (Li and Durbin 2009)	bio-bwa.sourceforge.net/
samtools	Github/open source	samtools.github.io
pairsamtools	Github/open source	github.com/mirnylab/pairsamtools
pairix	Github/open source	github.com/4dn-dcic/pairix
cooler	Abdennur, N., and Mirny, L. (Abdennur and Mirny 2020)	github.com/mirnylab/cooler
Miniconda	Anaconda	docs.conda.io/en/latest/miniconda.html
Snakemake	Github/open source	snakemake.github.io

Creation of *nhomie* deletion flies

To modify *nhomie* at the *eve* locus, we used recombinase-mediated cassette exchange (Bateman et al. 2006). First, we inserted two closely positioned attP sites, using CRISPR. The donor plasmid for this was constructed as follows. First, a mini-*white* (*mw*) gene with Glass binding sites (Fujioka et al. 1999) was inserted into BlueScript. From the standard *mw* gene, the Wari insulator (Chetverina et al. 2008) was deleted. Then, two 102bp attP sequences (Venken et al. 2011) were inserted, one just 5' of the Glass binding sites and the other at the 3' end of the modified *mw*, creating the plasmid P-attPx2-*mw*. 5'- and 3'-homologous arms were added to both ends. Two gRNA sequences were cloned into plasmid pCFD4 ((Port et al. 2014) (Addgene). The donor and gRNA plasmids were injected into a Cas9 line (y[1] M{vas-Cas9.S}ZH-2A w[1118], Bloomington Drosophila Stock Center). This chromosomal modification resulted in one attP site being inserted

in the intron of *CG12134*, and the other being inserted between the *eve* 7-stripe enhancer and the 3+7 stripe enhancer. This also deleted 2.2kb of endogenous sequence, including *nhomie* and the *eve* 7-stripe enhancer.

After identifying a successful insertion (NattPmw), *mw* was replaced by each of the following using RMCE: 1) the previously deleted 2.2kb, restoring *nhomie* and the *eve* 7-stripe enhancer, to create "wild-type *nhomie*" (*nhomie forward*), 2) the same 2.2kb sequence, but with 600bp of phage λ DNA in place of 600bp *nhomie* (*λ DNA*), 3) the same 2.2kb sequence, but with 600bp *nhomie* inverted (*nhomie reverse*), and 4) the same 2.2kb sequence, but with 600bp *nhomie* replaced by a copy of ~600bp *homie* in its native orientation in the chromosome (*homie forward*). Each of these changes was confirmed by sequencing of genomic DNA from the transgenic fly lines.

Analysis of embryonic cuticle patterns and *in situ* hybridization

To identify defects in developing embryos, embryos were collected for 2.5h, and allowed to develop for an additional 20-21h at 25°C. Embryos were dechorionated and mounted in a 1:1 mixture of Hoyer's medium and lactic acid. Mounted embryos were left at room temperature until they cleared (12-14 days), and the patterns of ventral abdominal denticles were examined and tallied as follows. Loss of at least one-fifth of a denticle band (in A1-A8) was counted as "missing". Fused denticle bands, which rarely occurred, was also counted as a "missing" band. Minor defects such as those within individual denticle rows were not counted.

Digoxigenin (DIG) *in situ* hybridization was performed using DIG-labeled anti-sense RNA against *CG12134*, *eIFj3*, and *TER94*. RNA expression was visualized using alkaline phosphatase-conjugated anti-DIG antibody (Roche), using CBIP and NBT as substrates (Roche). Each set of experiments was carried out in parallel to minimize experimental variation. Representative expression patterns are shown in each figure.

HCR-FISH

The sequences of target genes were obtained from Flybase (*flybase.org*)(Gramates et al. 2022). To design probes, the target gene sequences were submitted to the Molecular Instruments probe design platform (*www.molecularinstruments.com/hcr-rnafish*) (Choi et al. 2016), with parameters set to a 35 probe set size for *Drosophila melanogaster*. A similar method was designed based on published smFISH methods (Little and Gregor 2018; Trcek et al. 2017). 100-200 flies were placed in a cage with an apple juice plate at the bottom of the cage. For early stages, the embryos were collected for 7 hours, while for later-stage embryos, collections were overnight. Embryos from each plate were washed into collection mesh and dechorionated in bleach for 2min, then fixed in 5mL of 4% paraformaldehyde in 1X PBS and 5mL of heptane for 15min with horizontal shaking. The paraformaldehyde was then removed and replaced with 5mL methanol. The embryos were then devitellinized by vortexing for 30s, and washed in 1mL of methanol twice. Methanol was then removed and replaced by PTw (1X PBS with 0.1% Tween-20) through serial dilution as 7:3, 1:1, and 3:7 methanol:PTw. The embryos were washed twice in 1mL of PTw and pre-hybridized in 200μL of probe hybridization buffer for 30min at 37°C. 0.4pmol of each probe set were added to the embryos in the probe hybridization buffer, and the embryos were incubated at 37°C for 12-14h. The embryos were then washed 3X with probe wash buffer at 37°C for 30min and 2X with 5X SSCT(5X SSC+0.1% tween) at room temperature for 5min. Then the embryos were pre-amplified with 300μL amplification buffer for 10min at 25°C. Meanwhile, 6pmol of hairpin h1 and h2 were snap-cooled separately (95°C for 90s, cool to RT with 0.1°C drop per second), and then mixed in 100μL of amplification buffer at room temperature. After that, the pre-amplification solution was removed from the embryos, and 100μL of hairpin h1/h2 mix were added to the embryos. Next, the embryos were incubated for 12-14h at room temperature in the dark. To remove excess hairpins, the embryos were washed in SSCT as follows: 2X for 5min, 2X for 30min and 5X for 5min. Then, the embryos were washed with 1mL PTw for 2min and stained with

DAPI/Hoechst at 1µg/mL for 15min at room temperature in the dark. The embryos were then washed with PTw 3X for 5min. Finally, the embryos were mounted on microscope slides with Vectashield and a #1.5 coverslip for imaging.

Imaging, image analysis and statistics

Embryos from HCR-FISH were imaged using a Nikon A1 confocal microscope system, with a Plan Apo 20X/0.75 DIC objective. Z-stack images were taken at interval of 2µm, 4X average, 1024X1024 resolution, and the appropriate laser power and gain were set for 405, 488, 561, and 640 channels to avoid overexposure. Images were processed by ImageJ and the maximum projection was applied to each of the stack images. To determine the presence of stripes in early embryos, multi-channel images were first split into single channels and the stripe signal was highlighted and detected by the MaxEntropy thresholding method. GraphPad Prism was used for data visualization and statistical analysis. Two-way ANOVA with Tukey's multiple comparisons test for each pair of groups was used to determine the statistical significance for the percentage of embryos carrying stripes in *eIF3j* and *TER94* channels in each group.

MicroC library construction for the *nhomie* replacements

Embryos were collected on yeasted apple juice plates in population cages for 4h, incubated for 12h at 25°C, then subjected to fixation as follows. Embryos were dechorionated for 2min in 3% sodium hypochlorite, rinsed with deionized water, and transferred to glass vials containing 5mL PBST (0.1% Triton-X100 in PBS), 7.5mL n-heptane, and 1.5mL fresh 16% formaldehyde. Crosslinking was carried out at room temperature for exactly 15min on an orbital shaker at 250rpm, followed by addition of 3.7 mL 2M Tris-HCl pH7.5 and shaking for 5min to quench the reaction. Embryos were washed twice with 15mL PBST and subjected to secondary crosslinking. Secondary crosslinking was done in 10mL of freshly prepared 3mM final DSG and ESG in PBST for 45min at room temperature with passive mixing. The reaction was quenched by addition of 3.7mL of 2M Tris-HCl pH7.5 for 5min, washed twice with PBST, snap-frozen, and stored at -80°C until library construction.

Micro-C libraries were prepared as previously described (Batut et al. 2022) with the following modifications: 50µL of 12-16h embryos were used for each biological replicate. 60U of MNase was used for each reaction to digest chromatin to a mononucleosome:dinucleosome ratio of 4. Libraries were barcoded, pooled and subjected to paired-end sequencing on an Illumina Novaseq S1 100nt Flowcell (read length 50 bases per mate, 6-base index read).

Two or more independent biological replicates were sequenced for each genotype. For each replicate, >1000 embryos were used, and ~250M reads sequenced. Post-sequencing QC analysis was done for every sample, and the QC reports are available along with the sequence data in GEO(GSE263270). The raw sequencing data are also available in GSE263270 for use in further bioinformatics analysis. The figures present the merged data from all independent biological replicates for each genotype. The total read numbers in the merged data are very similar for each genotype (~500M reads).

MicroC data processing

MicroC data for *D. melanogaster* were aligned to custom genomes edited from the Berkeley Drosophila Genome Project (BDGP) Release 6 reference assembly (dos Santos et al. 2015) with BWA-MEM (Li and Durbin 2009) using parameters **-S -P -5 -M**. The resultant BAM files were parsed, sorted, de-duplicated, filtered, and split with Pairtools (*https://github.com/mirnylab/pairtools*). We removed pairs where only half of the pair could be mapped, or where the MAPQ score was less than three. The resultant files were indexed with Pairix (*https://github.com/4dn-dcic*

/pairix). The files from replicates were merged with Pairtools before generating 100bp contact matrices using Cooler (Abdennur and Mirny 2020). Finally, balancing and Mcool file generation was performed with Cooler's Zoomify tool.

Virtual 4C profiles were extracted from individual replicates using FAN-C (Kruse et al. 2020) at 400bp resolution. The values were summed across replicates and smoothed across three bins (1.2kb). The *homie* viewpoint was set to the 549nt *homie* sequence that was defined in previous studies (Fujioka et al. 2009).

Data availability

Sequence data are available at GEO(GSE263270). All confocal images are available upon request.

Figures Supplemental

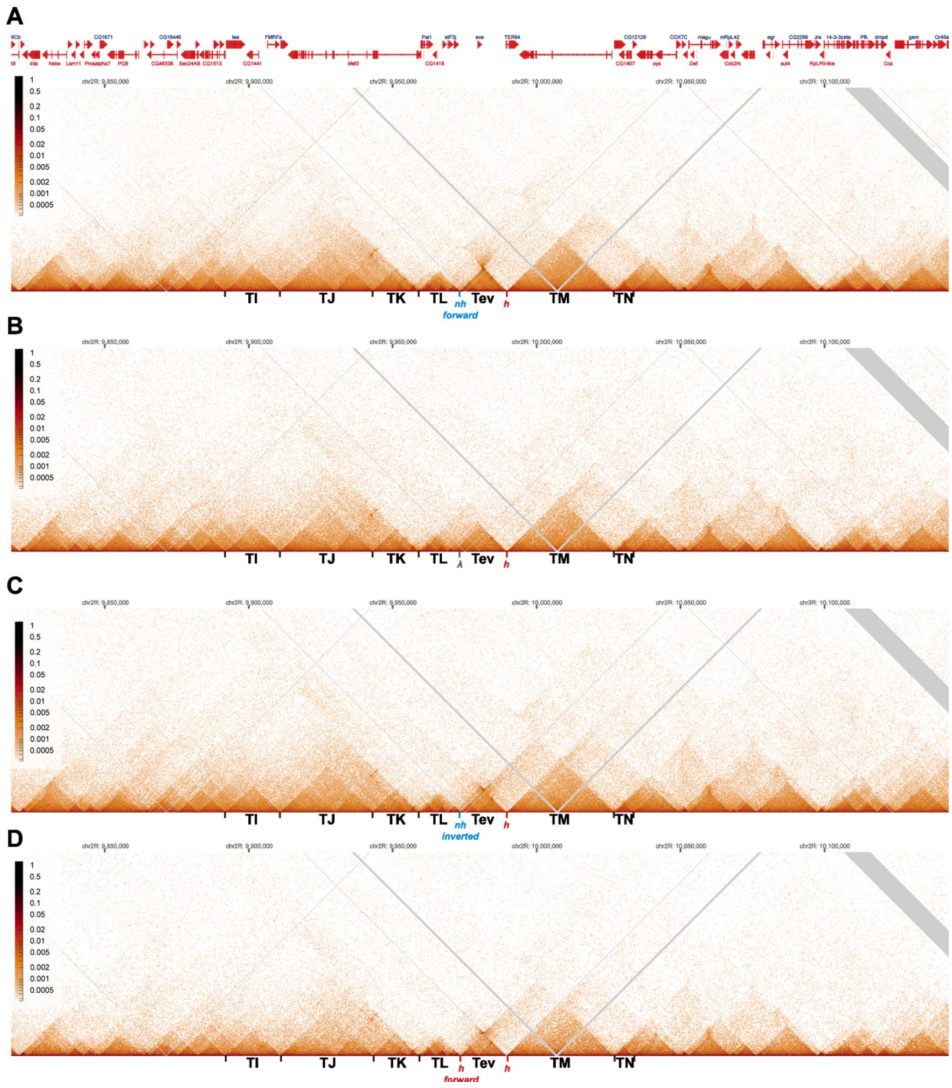

Fig. Supplemental 1.

MicroC contact profiles for *nhomie forward*, *lambda*, *nhomie reverse*, and *homie forward* in larger scale.

N (replicates) = 2. Resolution = 200. A) MicroC contact maps for the *nhomie forward* replacement. B) MicroC contact maps for the *lambda* replacement. C) MicroC profile of the *nhomie reverse* replacement. D) MicroC profile of the *homie forward* replacement.

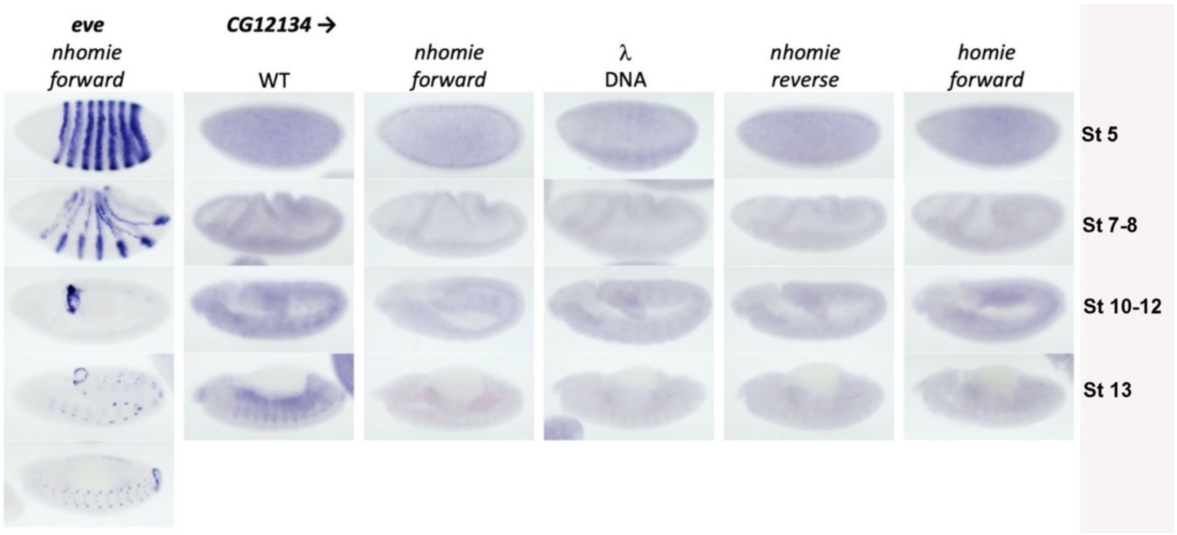

Fig. Supplemental 2.

Expression of *CG12134* in WT (*yw*) and the four *nhomie* replacements.

Digoxigenin *in situ* hybridization was used to detect expression of *CG12134* during development in the indicated genetic backgrounds. Approximate developmental stages of the embryos in each genetic background are shown on the right. As controls, embryos of similar stages were hybridized with an *eve* probe (top to bottom: stages 5, 7, 10, 11, and 13, respectively).

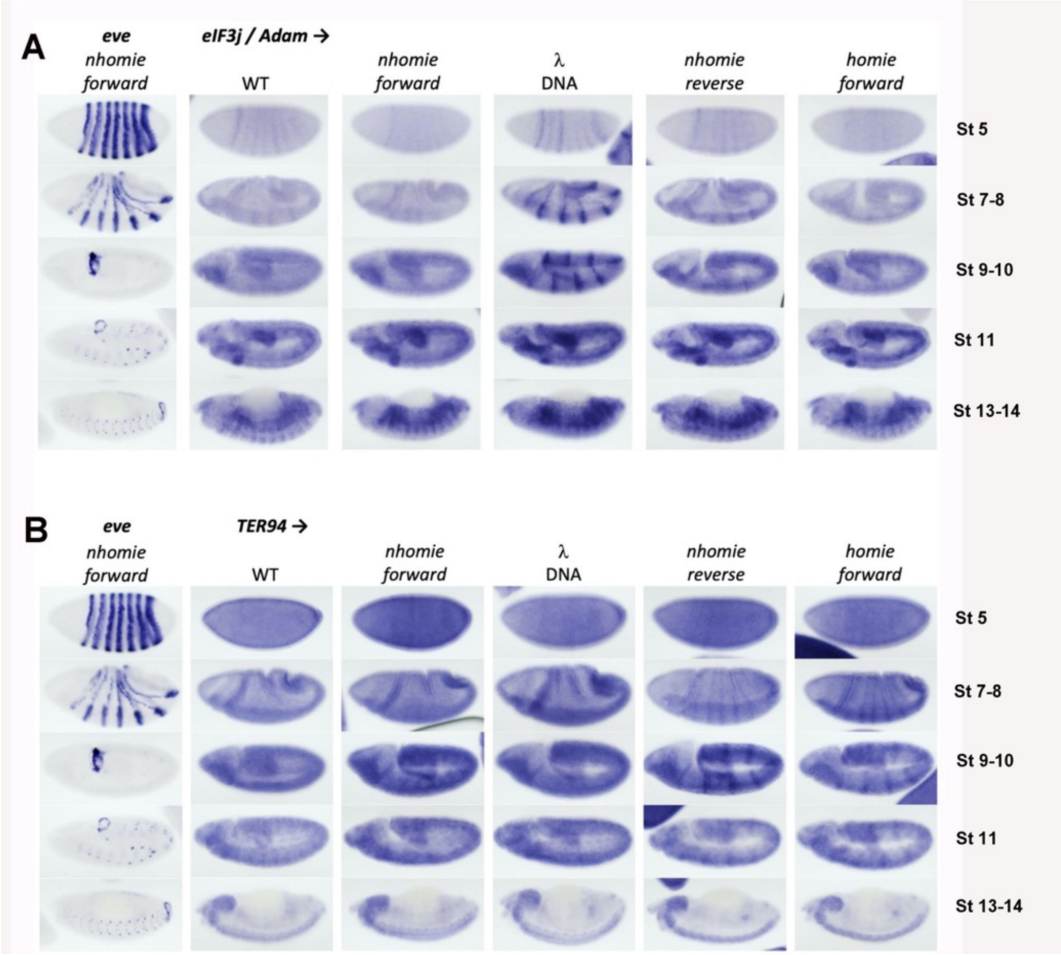

Fig. Supplemental 3.

Expression of *eIF3j* (*Adam*) and *TER94* in WT (*yw*) and the four *nhomie* replacements.

Digoxigenin *in situ* hybridization was used to detect expression of A) *eIF3j* and B) *TER94* during development in the indicated genetic backgrounds. Approximate developmental stages of the embryos in each genetic background are shown on the right. As controls, embryos of a similar stage were hybridized with an *eve* probe. Note that unlike the HCR-FISH results shown in **Fig. 4**, we can detect a low level of *eIF3j* stripe expression in WT (*yw*) and *nhomie forward* stage 5 embryos. The difference is likely due to the fact that signal amplification in the digoxigenin *in situ* hybridization procedure is non-linear, resulting in greater contrast between background and signal when staining conditions are optimal.

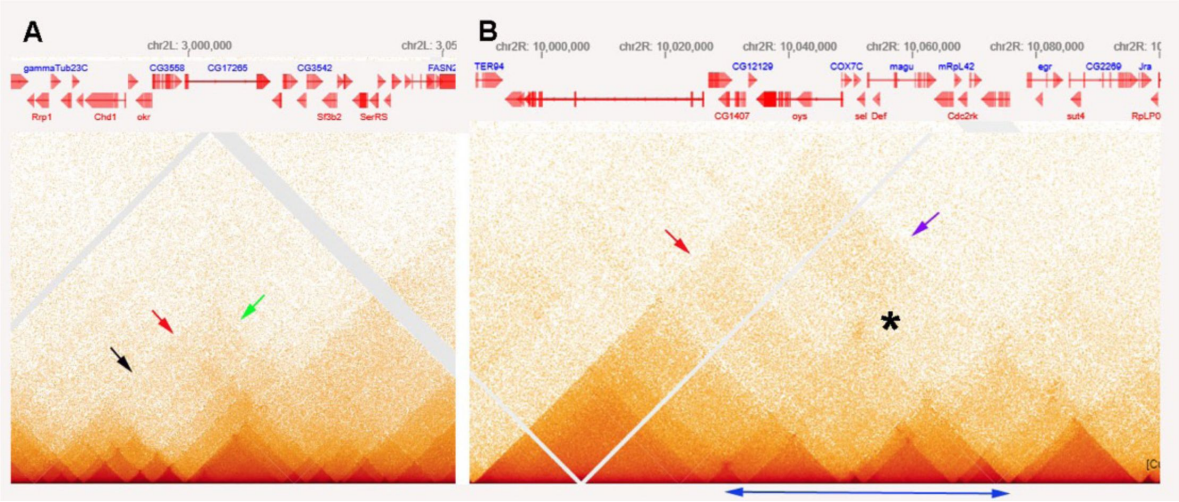

Fig. Supplemental 4.

MicroC patterns of DNA segments on the left and right arm of chromosome 2.

A) MicroC contact profiles of the left arm of chromosome 2 around 3,000,000 bp. The black arrow indicates where interactions between neighboring TADs are suppressed, as might be expected for a stem-loop configuration. The red arrow just above and to the right of the black arrow points to contacts between next-next-(next) door neighbors that are enhanced. However, the plume that is formed is one-sided, as indicated by the green arrow. B) MicroC contact profiles for TADs in a portion of the right arm of chromosome 2. The TADs indicated by the double-headed blue arrow at the bottom have a complex pattern of neighbor interactions. The asterisk and purple arrow indicate a potential volcano plume; however, unlike the *eve* volcano triangle and plume, this plume appears to be generated by crosslinking between sequences to either side of the collection of TADs indicated by the double-headed blue arrow. The TAD-to-TAD interaction patterns are further complicated by a band of enhanced crosslinking (red arrow).

References

Abdennur N, Mirny LA (2020) **Cooler: Scalable storage for hi-c data and other genomically labeled arrays** *Bioinformatics* **36**:311–316

Americo J, Whiteley M, Brown JL, Fujioka M, Jaynes JB, Kassis JA (2002) **A complex array of DNA-binding proteins required for pairing-sensitive silencing by a polycomb group response element from the drosophila engrailed gene** *Genetics* **160**:1561–1571

Arzate-Mejía RG, Josué Cerecedo-Castillo A, Guerrero G, Furlan-Magaril M, Recillas-Targa F (2020) **In situ dissection of domain boundaries affect genome topology and gene transcription in drosophila** *Nat Commun* **11**

Bateman JR, Lee AM, Wu CT (2006) **Site-specific transformation of drosophila via phic31 integrase-mediated cassette exchange** *Genetics* **173**:769–777

Batut PJ, Bing XY, Sisco Z, Raimundo J, Levo M, Levine MS (2022) **Genome organization controls transcriptional dynamics during development** *Science* **375**:566–570

Bell AC, West AG, Felsenfeld G (2001) **Insulators and boundaries: Versatile regulatory elements in the eukaryotic genome** *Science* **291**:447–450

Bing X, Ke W, Fujioka M, Kurbidaeva A, Levitt S, Levine M, Schedl P, Jaynes JB (2024) **Chromosome structure i: Loop extrusion or boundary:Boundary pairing?** *eLife. preprint* https://doi.org/10.7554/eLife.94070.1

Cai HN, Shen P (2001) **Effects of cis arrangement of chromatin insulators on enhancer-blocking activity** *Science* **291**:493–495

Cavalheiro GR, Pollex T, Furlong EE (2021) **To loop or not to loop: What is the role of tads in enhancer function and gene regulation?** *Curr Opin Genet Dev* **67**:119–129

Chen H, Levo M, Barinov L, Fujioka M, Jaynes JB, Gregor T (2018) **Dynamic interplay between enhancer–promoter topology and gene activity** *Nat Genet* **50**

Chetverina D, Aoki T, Erokhin M, Georgiev P, Schedl P (2014) **Making connections: Insulators organize eukaryotic chromosomes into independent cis-regulatory networks** *Bioessays* **36**:163–172

Chetverina D, Fujioka M, Erokhin M, Georgiev P, Jaynes JB, Schedl P (2017) **Boundaries of loop domains (insulators): Determinants of chromosome form and function in multicellular eukaryotes** *Bioessays* **39**

Chetverina D, Savitskaya E, Maksimenko O, Melnikova L, Zaytseva O, Parshikov A, Galkin AV, Georgiev P (2008) **Red flag on the white reporter: A versatile insulator abuts the white gene in drosophila and is omnipresent in mini-white constructs** *Nucleic Acids Res* **36**:929–937

Choi HM *et al.* (2016) **Mapping a multiplexed zoo of mrna expression** *Development* **143**:3632–3637

Davidson IF, Peters JM (2021) **Genome folding through loop extrusion by smc complexes** *Nat Rev Mol Cell Biol* **22**:445–464

dos Santos G, Schroeder AJ, Goodman JL, Strelets VB, Crosby MA, Thurmond J, Emmert DB, Gelbart WM, FlyBase C (2015) **Flybase: Introduction of the drosophila melanogaster release 6 reference genome assembly and large-scale migration of genome annotations** *Nucleic Acids Res* **43**:D690–697

Erokhin M *et al.* (2021) **Boundaries potentiate polycomb response element-mediated silencing** *BMC Biol* **19**

Fujioka M, Emi-Sarker Y, Yusibova GL, Goto T, Jaynes JB (1999) **Analysis of an even-skipped rescue transgene reveals both composite and discrete neuronal and early blastoderm enhancers, and multi-stripe positioning by gap gene repressor gradients** *Development* **126**:2527–2538

Fujioka M, Mistry H, Schedl P, Jaynes JB (2016) **Determinants of chromosome architecture: Insulator pairing in cis and in trans** *PLoS Genet* **12**

Fujioka M, Wu X, Jaynes JB (2009) **A chromatin insulator mediates transgene homing and very long-range enhancer-promoter communication** *Development* **136**:3077–3087

Fujioka M, Yusibova GL, Zhou J, Jaynes JB (2008) **The DNA-binding polycomb-group protein pleiohomeotic maintains both active and repressed transcriptional states through a single site** *Development* **135**:4131–4139

Goel VY, Huseyin MK, Hansen AS (2023) **Region capture micro-c reveals coalescence of enhancers and promoters into nested microcompartments** *Nat Genet* **55**:1048–1056

Gohl D, Aoki T, Blanton J, Shanower G, Kappes G, Schedl P (2011) **Mechanism of chromosomal boundary action: Roadblock, sink, or loop?** *Genetics* **187**:731–748

Gramates LS *et al.* (2022) **Flybase: A guided tour of highlighted features** *Genetics* **220**

Heger P, George R, Wiehe T (2013) **Successive gain of insulator proteins in arthropod evolution** *Evolution* **67**:2945–2956

Heger P, Wiehe T (2014) **New tools in the box: An evolutionary synopsis of chromatin insulators** *Trends Genet* **30**:161–171

Higashi TL, Uhlmann F (2022) **Smc complexes: Lifting the lid on loop extrusion** *Curr Opin Cell Biol* **74**:13–22

Hsieh TS, Cattoglio C, Slobodyanyuk E, Hansen AS, Rando OJ, Tjian R, Darzacq X (2020) **Resolving the 3d landscape of transcription-linked mammalian chromatin folding** *Mol Cell* **78**:539–553

Ibragimov A, Bing XY, Shidlovskii YV, Levine M, Georgiev P, Schedl P (2023) **Lncrna read-through regulates the bx-c insulator fub-1** *Elife* **12**

Jerković I, Szabo Q, Bantignies F, Cavalli G (2020) **Higher-order chromosomal structures mediate genome function** *J Mol Biol* **432**:676–681

Kassis JA, VanSickle EP, Sensabaugh SM (1991) **A fragment of engrailed regulatory DNA can mediate transvection of the white gene in drosophila** *Genetics* **128**:751–761

Kellum R, Schedl P (1992) **A group of scs elements function as domain boundaries in an enhancer-blocking assay** *Mol Cell Biol* **12**:2424–2431

Kerpedjiev P *et al.* (2018) **Higlass: Web-based visual exploration and analysis of genome interaction maps** *Genome Biol* **19**

Krietenstein N *et al.* (2020) **Ultrastructural details of mammalian chromosome architecture** *Mol Cell* **78**:554–565

Kruse K, Hug CB, Vaquerizas JM (2020) **Fan-c: A feature-rich framework for the analysis and visualisation of chromosome conformation capture data** *Genome Biol* **21**

Kyrchanova O, Chetverina D, Maksimenko O, Kullyev A, Georgiev P (2008) **Orientation-dependent interaction between drosophila insulators is a property of this class of regulatory elements** *Nucleic Acids Res* **36**:7019–7028

Kyrchanova O, Ivlieva T, Toshchakov S, Parshikov A, Maksimenko O, Georgiev P (2011) **Selective interactions of boundaries with upstream region of abd-b promoter in drosophila bithorax complex and role of dctcf in this process** *Nucleic Acids Res* **39**:3042–3052

Kyrchanova O, Kurbidaeva A, Sabirov M, Postika N, Wolle D, Aoki T, Maksimenko O, Mogila V, Schedl P, Georgiev P (2018) **The bithorax complex iab-7 polycomb response element has a novel role in the functioning of the fab-7 chromatin boundary** *PLoS Genet* **14**

Kyrchanova O, Toshchakov S, Podstreshnaya Y, Parshikov A, Georgiev P (2008) **Functional interaction between the fab-7 and fab-8 boundaries and the upstream promoter region in the drosophila abd-b gene** *Mol Cell Biol* **28**:4188–4195

Levo M, Raimundo J, Bing XY, Sisco Z, Batut PJ, Ryabichko S, Gregor T, Levine MS (2022) **Transcriptional coupling of distant regulatory genes in living embryos** *Nature* **605**:754–760

Li H, Durbin R (2009) **Fast and accurate short read alignment with burrows-wheeler transform** *Bioinformatics* **25**:1754–1760

Li H-B, Muller M, Bahechar IA, Kyrchanova O, Ohno K, Georgiev P, Pirrotta V (2011) **Insulators, not polycomb response elements, are required for long-range interactions between polycomb targets in drosophila melanogaster** *Mol Cell Biol* **31**:616–625

Little SC, Gregor T (2018) **Single mrna molecule detection in drosophila** *Methods Mol Biol* **1649**:127–142

Matthews NE, White R (2019) **Chromatin architecture in the fly: Living without ctcf/cohesin loop extrusion?** *BioEssays* **9**

Mohana G *et al.* (2023) **Chromosome-level organization of the regulatory genome in the drosophila nervous system** *Cell* **186**:3826–3844

Muller M, Hagstrom K, Gyurkovics H, Pirrotta V, Schedl P (1999) **The mcp element from the drosophila melanogaster bithorax complex mediates long-distance regulatory interactions** *Genetics* **153**:1333–1356

Muravyova E, Golovnin A, Gracheva E, Parshikov A, Belenkaya T, Pirrotta V, Georgiev P (2001) **Loss of insulator activity by paired su(hw) chromatin insulators** *Science* **291**:495–498

Perea-Resa C, Wattendorf L, Marzouk S, Blower MD (2021) **Cohesin: Behind dynamic genome topology and gene expression reprogramming** *Trends Cell Biol* **31**:760–773

Port F, Chen H-M, Lee T, Bullock SL (2014) **Optimized crispr/cas tools for efficient germline and somatic genome engineering in drosophila** *Proceedings of the National Academy of Sciences* **111**:E2967–E2976

Rowley MJ, Corces VG (2018) **Organizational principles of 3d genome architecture** *Nature Reviews Genetics* **19**:789–800

Schindelin J *et al.* (2012) **Fiji: An open-source platform for biological-image analysis** *Nat Methods* **9**:676–682

Schoborg TA, Labrador M (2010) **The phylogenetic distribution of non-ctcf insulator proteins is limited to insects and reveals that beaf-32 is drosophila lineage specific** *J Mol Evol* **70**:74–84

Sigrist CJ, Pirrotta V (1997) **Chromatin insulator elements block the silencing of a target gene by the drosophila polycomb response element (pre) but allow trans interactions between pres on different chromosomes** *Genetics* **147**:209–221

Stadler MR, Haines JE, Eisen MB (2017) **Convergence of topological domain boundaries, insulators, and polytene interbands revealed by high-resolution mapping of chromatin contacts in the early drosophila melanogaster embryo** *eLife* **6**

Trcek T, Lionnet T, Shroff H, Lehmann R (2017) **Mrna quantification using single-molecule fish in drosophila embryos** *Nat Protoc* **12**:1326–1348

Vazquez J *et al.* (1993) **Genetic and molecular analysis of chromatin domains** *Cold Spring Harb Symp Quant Biol* **58**:45–54

Vazquez J, Muller M, Pirrotta V, Sedat JW (2006) **The mcp element mediates stable long-range chromosome-chromosome interactions in drosophila** *Molecular Biology of the Cell* **17**:2158–2165

Venken KJT *et al.* (2011) **Mimic: A highly versatile transposon insertion resource for engineering drosophila melanogaster genes** *Nat Methods* **8**:737–743

Yokoshi M, Segawa K, Fukaya T (2020) **Visualizing the role of boundary elements in enhancer-promoter communication** *Mol Cell* **78**:224–235

Editors

Reviewing Editor
Yukiko Yamashita
Whitehead Institute/MIT, Cambridge, United States of America

Senior Editor
Claude Desplan
New York University, New York, United States of America

Reviewer #1 (Public Review):

In this study, the authors engineer the endogenous left boundary of the Drosophila eve TAD, replacing the endogenous Nhomie boundary by either a neutral DNA, a wildtype Nhomie boundary, an inverted Nhomie boundary, or a second copy of the Homie boundary. They perform Micro-C on young embryos and conclude that endogenous Nhomie and Homie boundaries flanking eve pair with head-to-tail directionality to form a chromosomal stem loop. Abrogating the Nhomie boundary leads to ectopic activation of genes in the former neighboring TAD by eve embryonic stripe enhancers. Replacing Nhomie by an inverted version or by Homie (which pairs with itself head-to-head) transformed the stem loop into a circle loop. An important finding was that stem and circle loops differentially impact endogenous gene regulation both within the eve TAD and in the TADs bracketing eve. Intriguingly, an eve TAD with a circle loop configuration leads to ectopic activation of flanking genes by eve enhancers - indicating compromised regulatory boundary activity despite the presence of an eve TAD with intact left and right boundaries.

The results obtained are of high-quality and are meticulously discussed. This work advances our fundamental understanding of how 3D genome topologies affect enhancer-promoter communication.

This study raises interesting questions to be addressed in future studies.

First, given the unique specificity with which Nhomie and Homie pair (and exhibit "homing" activity), the generalizability of TAD formation by directional boundary pairing remains unclear. Testing whether boundary pairing is a phenomenon restricted to exceptional loci picked for study, rather than a broader rule of TAD formation, would best be done through the development of untargeted approaches to study boundary pairing.

Second, boundary pairing is one of several mechanisms that may form chromosomal contact domains such as TADs. Other mechanisms include cohesin-mediated chromosomal loop extrusion and the inherent tendency of transcriptionally active and inactive chromatin to segregate (or compartmentalize). The functional interplay between these possible TAD-forming mechanisms remains to be further investigated.

https://doi.org/10.7554/eLife.94114.2.sa1

Reviewer #2 (Public Review):

This study reports a set of experiments and subsequent analyses focusing on the role of Drosophila boundary elements in shaping 3D genome structure and regulating gene expression. The authors primarily focus on the region of the fly genome containing the even skipped (eve) gene; eve is expressed in a canonical spatial pattern in fly embryos and its locus is flanked by the well-characterized neighbor of homie (nhomie) and homie boundary elements. The main focus of the investigation is the orientation dependence of these boundary elements, which had been observed previously using reporter assays. In this study, the authors use Crispr/Cas9 editing followed by recombination-mediated cassette exchange to create a series of recombinant fly lines in which the nhomie boundary element is either replaced with exongenous sequence from phage λ, an inversion of nhomie, or a copy of homie that has the same orientation as the endogenous homie sequence. The nhomie sequence is also regenerated in its native orientation to control for effects introduced by the transgenesis process.

The authors then perform high-resolution Micro-C to analyze 3D structure and couple this with fluorescent and colorimetric RNA in situ hybridization experiments to measure the expression of eve and nearby genes during different stages of fly development. The major

findings of these experiments are that total loss of boundary sequence (replacement with λ DNA) results in major 3D structure changes and the most prominent observed gene changes, while inversion of the nhomie boundary or replacement with homie resulted in more modest effects in terms of 3D structure and gene expression changes and a distinct pattern of gene expression change from the λ DNA replacement. As the samples in which the nhomie boundary is inverted or replaced with homie have similar Micro-C profiles at the eve locus and show similar patterns of a spurious gene activation relative to the control, the observed effects appear to be driven by the relative orientation of the nhomie and homie boundary elements to one another.

Collectively, the findings reported in the manuscript are of broad interest to the 3D genome field. Although extensive work has gone into characterizing the patterns of 3D genome organization in a whole host of species, the underlying mechanisms that structure genomes and their functional consequences are still poorly understood. The perhaps best understood system, mechanistically, is the coordinated action of CTCF with the cohesin complex, which in vertebrates appears to shape 3D contact maps through a loop extrusion-pausing mechanism that relies on orientation-dependent sequence elements found at the boundaries of interacting chromatin loops. Despite having a CTCF paralog and cohesin, the Drosophila genome does not appear to be structured by loop extrusion-pausing. The identification of orientation-dependent elements with pronounced structural effects on genome folding thus may shed light on alternative mechanisms used to regulated genome structure, which in turn may yield insights into the significance of particular folding patterns.

On the whole, this study is comprehensive and represents a useful contribution to the 3D genome field. The transgenic lines and Micro-C datasets generated in the course of the work will be valuable resources for the research community. Moreover, the manuscript, while dense in places, is generally clearly written and comprehensive in its description of the work. However, I have a number of comments and critiques of the manuscript, mainly centering on the framing of the experiments and presentation of the Micro-C results and on the manner in which the data are analyzed and reported.

As this document now reflects my review of a revised version of the initial preprint, I will begin to add the new content at this point. As discussed in detail in the following paragraphs, my initial impression of the manuscript has not changed, so I have accordingly left the above text unaltered.

In my initial review, I provided a number of suggestions to improve the quality of the manuscript. These suggestions, which took the form of six major and three minor points, largely focused on 1) altering the writing in certain places to make the story more broadly accessible to the readership and 2) the inclusion of key, missing methodological detail to increase the rigor and reproducibility of the study. No new experiments were requested, and all of the points could be readily addressed with rather straightforward textual changes.

In their revised manuscript, the authors elected to directly address one of the major points and two of the minor points (major point 4, minor points 1 and 3). The remainder of my suggestions remain entirely unaddressed. A similar level of responsiveness was afforded to the very reasonable critiques of the other Reviewer and the Reviewing Editor. The authors have instead largely chosen to respond to the points raised exclusively in the rebuttal document. This document sprawls across >22 pages, includes numerous in-line figures, and cites dozens of references. The tone of this document, in many places, is at best forceful. In a less generous interpretation, many sections are combative, dismissive, and borderline unprofessional.

It is my opinion that the authors are doing the scientific community a disservice with their response. While it is my understanding that readers will be able see the rebuttal letter, I find that end result far from satisfying. How many readers will take the trouble to access that file,

versus the manuscript itself? Skirting the review critiques places an unfair burden on readers, who are expecting peer-reviewed science, to dig into the accessory files to follow the critique and response, rather than seeing in reflected in the final product as they accustomed. Intentionally or not, the tactics the authors have chosen detract from what is otherwise a novel and well-intentioned new publishing model. It is also worth pointing out that peer review is done as an act of service to the scientific community, as the senior authors are doubtless aware. The other reviewer, the Reviewing Editor, and I have all taken time away from advancing our own careers and those of our trainees to offer the thoughtful critiques that were so pointedly dismissed.

In summary, as the vast majority of my critiques remain unaddressed, I have simply reproduced them below.

Major Points:

(1) The authors motivate much of the introduction and results with hypothetical "stem loop" and "circle loop" models of chromosome confirmation, which they argue are reflected in the Micro-C data and help to explain the observed ISH patterns. While such structures may possibly form, the support for these specific models vs. the many alternatives is not in any way justified. For instance, no consideration is given to important biophysical properties such as persistence length, packing/scaling, and conformational entropy. As the biophysical properties of chromatin are a very trafficked topic both in terms of experimentation and computational modeling and generally considered in the analysis of chromosome conformation data, the study would be strengthened by acknowledgement of this body of work and more direct integration of its findings.

(2) Similar to Point 1, while there is a fair amount of discussion of how the observed results are or are not consistent with loop extrusion, there is no discussion of the biophysical forces that are thought to underly compartmentalization such as block-polymer co-segregation and their potential influence. I found this absence surprising, as it is generally accepted that A/B compartmentalization essentially can explain the contact maps observed in Drosophila and other non-vertebrate eukaryotes (Rowley, ..., Corces 2017; PMID 28826674). The manuscript would be strengthened by consideration of this phenomenon.

(3) The contact maps presented in the study represent many cells and distinct cell types. It is clear from single-cell Hi-C and multiplexed FISH experiments that chromosome conformation is highly variable even within populations of the same cell, let alone between cell types, with structures such as TADs being entirely absent at the single cell level and only appearing upon pseudobulking. It is difficult to square these observations with the models of relatively static structures depicted here. The authors should provide commentary on this point.

(4) Related to Point 4, the lack of quantitative details about the Micro-C data make it difficult to evaluate if the changes observed are due to biological or technical factors. It is essential that the authors provide quantitative means of controlling for factors like sampling depth, normalization, and data quality between the samples.

(5) The ISH effects reported are modest, especially in the case of the HCR. The details provided for how the imaging data were acquired and analyzed are minimal, which makes evaluating them challenging. It would strengthen the study to provide much more detail about the acquisition and analysis and to include depiction of intermediates in the analysis process, e.g. the showing segmentation of stripes.

https://doi.org/10.7554/eLife.94114.2.sa0

Author response:

The following is the authors' response to the original reviews.

> ***Public Reviews:***
>
> ***Reviewer #1 (Public Review):***
>
> *Summary:*
>
> *In this study, the authors engineer the endogenous left boundary of the Drosophila eve TAD, replacing the endogenous Nhomie boundary by either a neutral DNA, a wildtype Nhomie boundary, an inverted Nhomie boundary, or a second copy of the Homie boundary. They perform Micro-C on young embryos and conclude that endogenous Nhomie and Homie boundaries flanking eve pair with head-to-tail directionality to form a chromosomal stem loop. Abrogating the Nhomie boundary leads to ectopic activation of genes in the former neighboring TAD by eve embryonic stripe enhancers. Replacing Nhomie by an inverted version or by Homie (which pairs with itself head-to-head) transformed the stem loop into a circle loop. An important finding was that stem and circle loops differentially impact endogenous gene regulation both within the eve TAD and in the TADs bracketing eve. Intriguingly, an eve TAD with a circle loop configuration leads to ectopic activation of flanking genes by eve enhancers - indicating compromised regulatory boundary activity despite the presence of an eve TAD with intact left and right boundaries.*
>
> *Strengths:*
>
> *Overall, the results obtained are of high-quality and are meticulously discussed. This work advances our fundamental understanding of how 3D genome topologies affect enhancer-promoter communication.*
>
> *Weaknesses:*
>
> *Though convincingly demonstrated at eve, the generalizability of TAD formation by directional boundary pairing remains unclear, though the authors propose this mechanism could underly the formation of all TADs in Drosophila and possibly even in mammals. Strong and ample evidence has been obtained to date that cohesin-mediated chromosomal loop extrusion explains the formation of a large fraction of TADs in mammals.*

(1.1) The difficultly with most all of the studies on mammal TADs, cohesin and CTCF roadblocks is that the sequencing depth is not sufficient, and large bin sizes (>1 kb) are needed to visualize chromosome architecture. The resulting contact profiles show TAD neighborhoods, not actual TADs.

The problem with these studies is illustrated by comparing the contact profiles of mammalian MicroC data sets at different bin sizes in Author response image 1. In this figure, the darkness of the "pixels" in panels E, F, G and H was enhanced by reducing brightness in photoshop.

Author response image 1.

Mammalian MicroC profiles different bun sizes

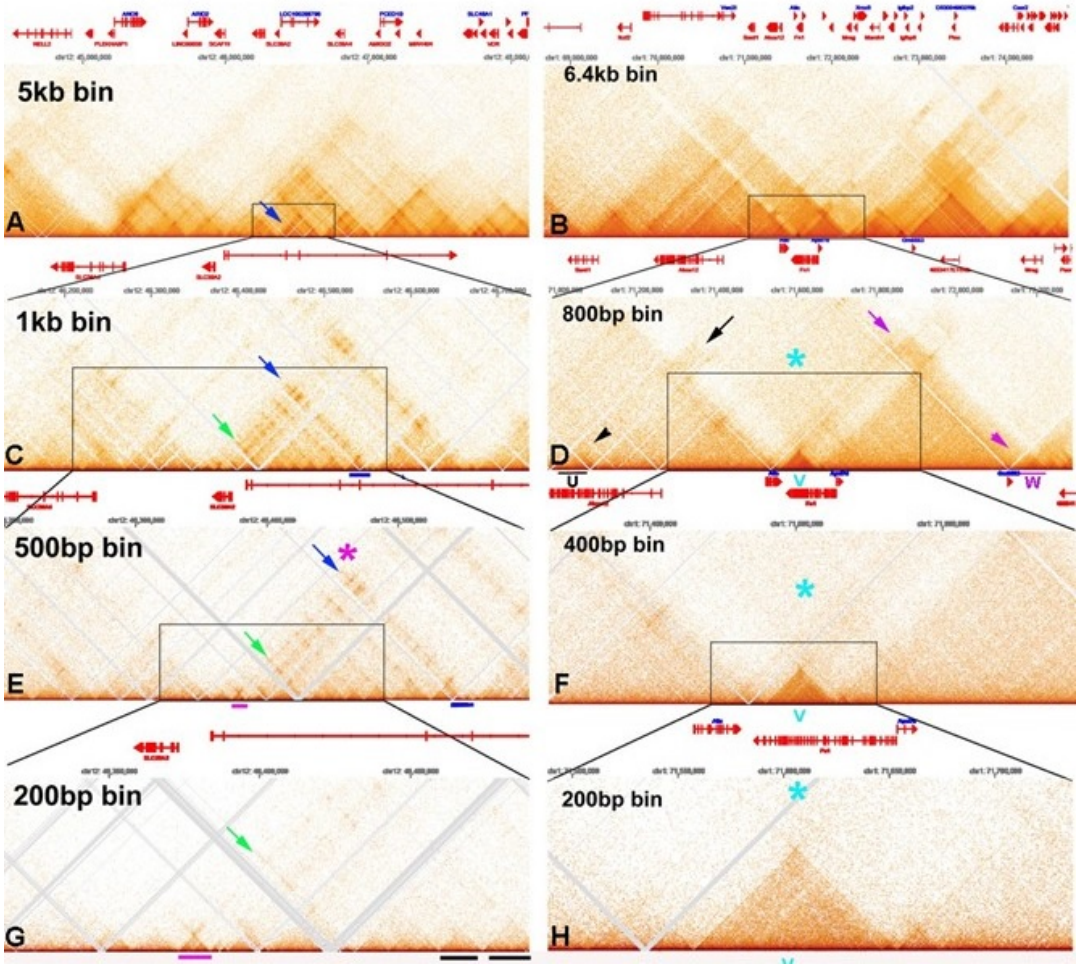

Panels A and C show “TADs” using bin sizes typical of most mammalian studies (see Krietenstein et al. (2023) (Krietenstein et al. 2020)). At this level of resolution, TADs, the “trees” that are the building blocks of chromosomes, are not visible. Instead, what is seen are TAD neighborhoods or “forests”. Each neighborhood consists of several dozen individual TADs. The large bins in these panels also artificially accentuated TAD:TAD interactions, generating a series of “stripes” and “dots” that correspond to TADs bumping into each other and sequences getting crosslinked. For example, in panel A there is prominent stripe on the edge of a “TAD” (blue arrow). In panel C, this stripe resolves into a series of dots arranged as parallel, but interrupted “stripes” (green and blue arrows). At the next level of resolution, it can be seen that the stripe marked by the blue arrow and magenta asterisk is generated by contacts between the left boundary of the TAD indicated by the magenta bar with sequences in a TAD (blue bar) ~180 kb way. While dots and stripes are prominent features in contact profiles visualized with larger bin sizes (A and C), the actual TADs that are observed with a bin size of 200 bp (examples are underlined by black bars in panel G) are not bordered by stripes, nor are they topped by obvious dots. The one possible exception is the dot that appears at the top of the volcano triangle underlined with magenta.

The chromosome 1 DNA segment from the MicroC data of Hseih et al. (2023) (Hsieh et al. 2020) shows a putative volcano triangle with a plume (indicated by a V in Author response image 1 panels D, F and H). Sequences in the V TAD don’t crosslink with their immediate neighbors, and this gives a “plume” above the volcano triangle, as indicate by the light blue asterisk in panels D, F and H. Interestingly the V TAD does contact two distant TADs, U on the left and W on the right. The U TAD is ~550 kb from V, and the region of contact is indicated by

the black arrow. The W TAD is ~585 kb from V, and the region of contact is indicated by the magenta arrow. While the plume still seems to be visible with a bin size of 400 bp (light blue asterisk), it is hard to discern when the bin size is 200 bp, as there are not enough reads.

The evidence demonstrating that cohesin is required for TAD formation/maintenance is based on low resolution Hi-C data, and the effects that are observed are on TAD neighborhoods (forests) and not TADs (trees). In fact, there is published evidence that cohesin is not required in mammals for TAD formation/maintenance. In an experiment from Goel et al. 2023 the authors depleted the cohesin component Rad21 and then visualized the effects on TAD organization using the high resolution region capture MicroC (RCMC) protocol. The MicroC contact map in this figure visualizes a ~250 kb DNA segment around the *Ppm1pg* locus at 250 bp resolution. On the right side of the diagonal is the untreated control, while the left side shows the MicroC profile of the same region after Rad21 depletion. The authors indicated that there was a 97% depletion of Rad21 in their experiment. However, as is evident from a comparison of the experimental and control, loss of Rad21 has no apparent effect on the TAD organization of this mammalian DNA segment.

Several other features are worth noting. First, unlike the MicroC experiments shown in Author response image 1, there are dots at the apex of the TADs in this chromosomal segment. In the MicroC protocol, fixed chromatin is digested to mononucleosomes by extensive MNase digestion. The resulting DNA fragments are then ligated, and dinucleosome-length fragments are isolated and sequenced.

DNA sequences that are nucleosome free in chromatin (which would be promoters, enhancers, silencers and boundary elements) are typically digested to oligonucleotides in this procedure and won't be recovered. This means that the dots shown here must correspond to mononucleosome-length elements that are MNase resistant. This is also true for the dots in the MicroC contact profiles of the *Drosophila Abd-B* regulatory domain (see Fig. 2B in the paper). Second, the TADs are connected to each other by 45o stripes (see blue and green arrowheads). While it is not clear from this experiment whether the stipes are generated by an active mechanism (enzyme) or by some "passive" mechanism (e.g., sliding), the stripes in this chromosomal segment *are not* generated by cohesin, as they are unperturbed by Rad21 depletion. Third, there are no volcano triangles with plumes in this chromosomal DNA segment. Instead, the contact patterns (purple and green asterisks) between neighboring TADs closely resemble those seen for the *Abd-B* regulatory domains (compare Goel et al. 2023 with Fig. 2B in the paper). This similarity suggests that the TADs in and around *Ppm1g* may be circle-loops, not stem-loops. As volcano triangles with plumes also seem to be rare in the MicroC data sets of Krietenstein et al. (Krietenstein et al. 2020) and Hesih et al. (Hsieh et al. 2020) (with the caveat that these data sets are low resolution: see Author response image 1), it is possible that much of the mammalian genome is assembled into circle-loop TADs, a topology that can't be generated by the cohesin loop extrusion (bolo tie clip) /CTCF roadblock model.

While Rad21 depletion has no apparent effect on TADs, it does appear to impact TAD neighborhoods. This is in a supplemental figure in Goel et al. (Goel et al. 2023). In this figure, TADs in the *Ppm1g* region of chromosome 5 are visualized with bin sizes of 5 kb and 1 kb. A 1.2 Mb DNA segment is shown for the 5 kb bin size, while an 800 kb DNA segment is shown for the 1 kb bin size. As can be seen from comparing the MicroC profiles in Author response image 2 with that in Goel et al. 2023, individual TADs are not visible. Instead, the individual TADs are binned into large TAD "neighborhoods" that consist of several dozen or more TADs.

Unlike the individual TADs shown in Goel et al. 2023, the TAD neighborhoods in Author response image 2 are sensitive to Rad21 depletion. The effects of Rad21 depletion can be seen by comparing the relative pixel density inside the blue lines before (above the diagonal) and after (below the diagonal) auxin-induced Rad21 degradation. The reduction in pixel density is greatest for more distant TAD:TAD contacts (farthest from the diagonal). By contrast, the TADs

themselves are unaffected (Goel et al. 2023), as are contacts between individual TADs and their immediate neighbors. In addition, contacts between partially overlapping TAD neighborhoods are also lost. At this point it isn't clear why contacts between distant TADs in the same neighborhood are lost when Rad21 is depleted; however, a plausible speculation is that it is related to the functioning of cohesin in holding newly replicated DNAs together until mitosis and whatever other role it might have in chromosome condensation.

Author response image 2.

Ppm1g full locus chr5

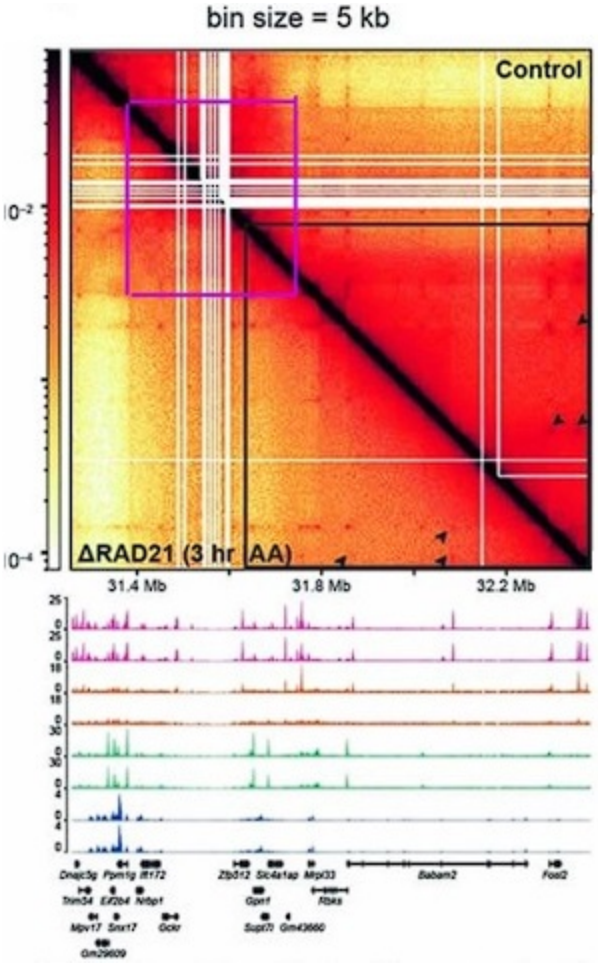

> *Moreover, given the unique specificity with which Nhomie and Homie are known to pair (and exhibit "homing" activity), it is conceivable that formation of the eve TAD by boundary pairing represents a phenomenon observed at exceptional loci rather than a universal rule of TAD formation. Indeed, characteristic Micro-C features of the eve TAD are only observed at a restricted number of loci in the fly genome.....*

(1.2) The available evidence does not support the claim that *nhomie* and *homie* are "exceptional." To begin with, *nhomie* and *homie* rely on precisely the same set of factors that have been implicated in the functioning of other boundaries in the fly genome. For example, *homie* requires (among other factors) the generic boundary protein Su(Hw) for insulation and long-distance interactions (Fujioka et al. 2024). (This is also true of *nhomie*: unpublished data.) The Su(Hw) protein (like other fly polydactyl zinc finger proteins) can engage in distant interactions. This was first shown by Sigrist and Pirrotta (Sigrist and Pirrotta 1997), who

found that the *su(Hw)* element from the *gypsy* transposon can mediate long-distance regulatory interactions (PRE dependent silencing) between transgenes inserted at different sites on homologous chromosomes (*trans* interactions) and at sites on different chromosomes.

The ability to mediate long-distance interactions is not unique to the su(Hw) element, or homie and nhomie. Muller et al. (Muller et al. 1999) found that the Mcp boundary from the Drosophila BX-C is also able to engage in long-distance regulatory interactions—both PRE-dependent silencing of mini-white and enhancer activation of mini-white and yellow. The functioning of the Mcp boundary depends upon two other generic insulator proteins, Pita and the fly CTCF homolog (Kyrchanova et al. 2017). Like Su(Hw) both are polydactyl zinc finger proteins, and they resemble the mammalian CTCF protein in that their N-terminal domain mediates multimerization (Bonchuk et al. 2020; Zolotarev et al. 2016). Figure 6 from Muller et el. 1999 shows PRE-dependent “pairing sensitive silencing” interactions between transgenes carrying a mini-white reporter, the Mcp and scs’ (Beaf dependent)(Hart et al. 1997) boundary elements, and a PRE closely linked to Mcp. In this experiment flies homozygous for different transgene inserts were mated and the eye color was examined in their transheterozygous progeny. As indicated in the figure, the strongest trans-silencing interactions were observed for inserts on the same chromosomal arm; however, transgenes inserted on the left arm of chromosome 3 can interact across the centromere with transgenes inserted on the right arm of chromosome 3.

Figure 5C (left) from Muller et el. 1999 shows a *trans*-silencing interaction between *w#11.102* at 84D and *w#11.16* approximately 5.8 Mb away, at 87D. Figure 5C (right) shows a *trans*-silencing interaction across the centromere between *w#14.29* on the left arm of chromosome 3 at 78F and *w#11.102* on the right arm of chromosome 3 at 84D. The eye color phenotype of *mini-white*-containing transgenes is usually additive: homozygyous inserts have twice as dark eye color as the corresponding hemizygous inserts. Likewise, in flies _trans-_heterozygous for *mini-white* transgenes inserted at different sites, the eye color is equivalent to the sum of the two transgenes. This is not true when *mini-white* transgenes are silenced by PREs. In the combination shown in panel A, the t_rans-_heterozygous fly has a lighter eye color than either of the parents. In the combination in panel B, the _trans-_heterozygous fly is slightly lighter than either parent.

As evident from the diagram in Figure 6 from Muller et el. 1999, all of the transgenes inserted on the 3rd chromosome that were tested were able to participate in long distance (>Mbs) regulatory interactions. On the other hand, not all possible pairwise interactions are observed. This would suggest that potential interactions depend upon the large scale (Mb) 3D folding of the 3rd chromosome.

When the scs boundary (Zw5 dependent) (Gaszner et al. 1999) was added to the transgene to give sMws’, it further enhanced the ability of distant transgenes to find each other and pair. All eight of the sMws’ inserts that were tested were able to interact with at least one other sMws’ insert on a different chromosome and silence mini-white. Vazquez et al. () subsequently tagged the sMws’ transgene with LacO sequences (ps0Mws’) and visualized pairing interactions in imaginal discs. Trans-heterozygous combinations on the same chromosome were found paired in 94-99% of the disc nuclei, while a trans-heterozygous combination on different chromosomes was found paired in 96% of the nuclei (Table 3 from Vazquez et al. 2006). Vazquez et al. also examined a combination of four transgenes inserted on the same chromosome (two at the same insertion site, and two at different insertion sites). In this case, all four transgenes were clustered together in 94% of the nuclei (Table 3 from Vazquez et al. 2006). Their studies also suggest that the distant transgenes remain paired for at least several hours. A similar experiment was done by Li et al. (Li et al. 2011), except that the transgene contained only a single boundary, Mcp or Fab-7. While pairing was still observed in trans-heterozygotes, the frequency was reduced without scs and scs’.

It is worth pointing out that there is no plausible mechanism in which cohesin could extrude a loop through hundreds of intervening TADs, across the centromere (*ff#13.101*ßà*w#11.102*: Figure 6 from Muller et el. 1999; *w#14.29*ßà*w#11.02*: Figure 6 from Muller et el. 1999 and 5) and come to a halt when it “encounters” *Mcp* containing transgenes on different homologs. The same is true for *Mcp*-dependent pairing interactions in *cis* (Fig. 7 in Muller et al. (Muller et al. 1999)) or *Mcp*-dependent pairing interactions between transgenes inserted on different chromosomes (Fig. 8 in Muller et al. (Muller et al. 1999); Line 8 in Table 3 from Vazquez et al. 2006).

These are not the only boundaries that can engage in long-distance pairing. Mohana et al. (Mohana et al. 2023) identified nearly 60 meta-loops, many of which appear to be formed by the pairing of TAD boundary elements. Two examples (at 200 bp resolution from 12-16 hr embryos) are shown in Author response image 3.

Author response image 3.

Metaloops on the 2nd and 3rd chromosomes: circle-loops and multiple stem-loops

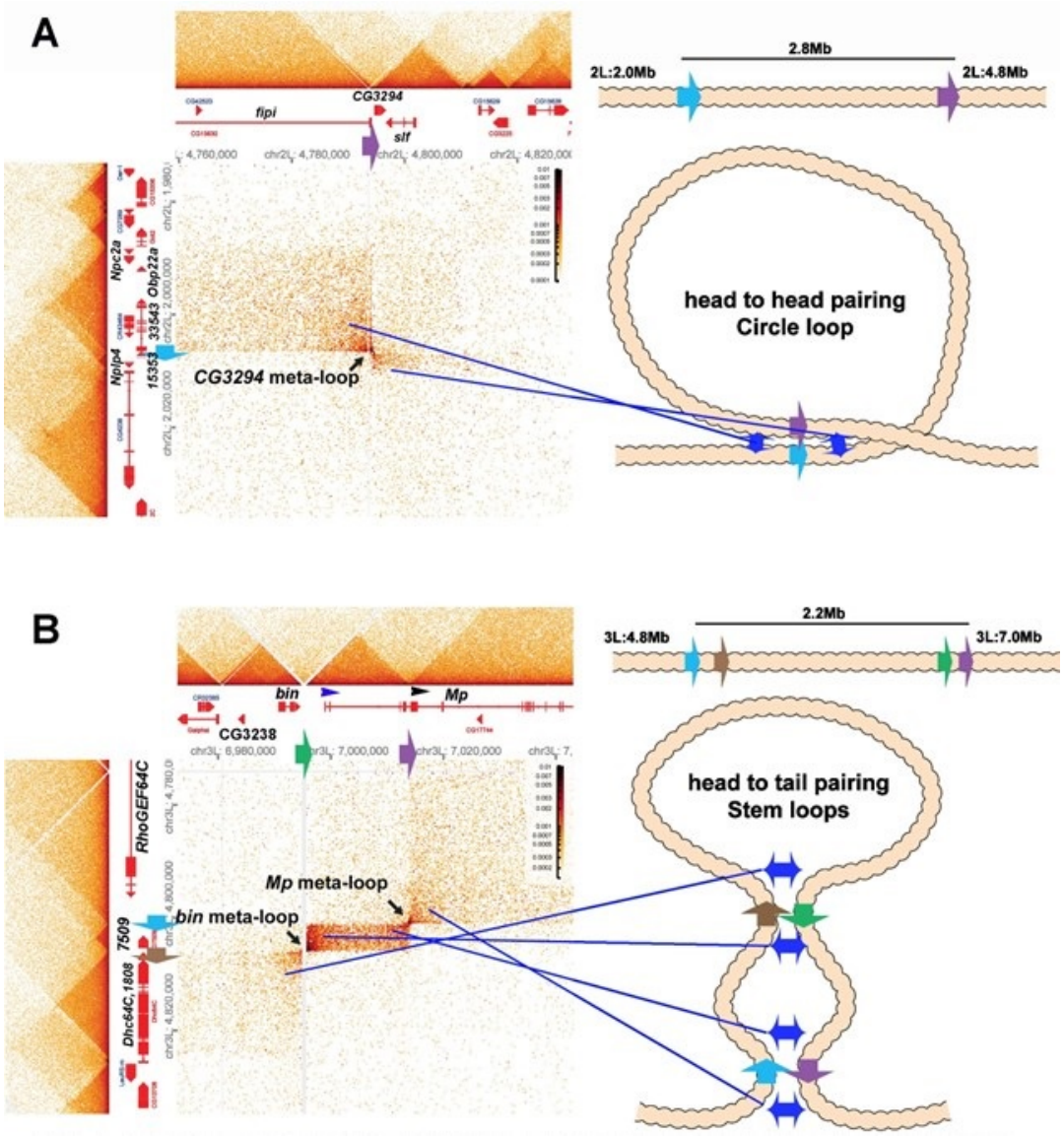

One of these meta-loops (panel A) is generated by the pairing of two TAD boundaries on the 2nd chromosome. The first boundary, blue, (indicated by blue arrow) is located at ~2,006, 500 bp between a small TAD containing the *Nplp4* and *CG15353* genes and a larger TAD containing 3 genes, *CG33543*, *Obp22a* and *Npc2a*. *Nplp4* encodes a neuropeptide. The functions of *CG15354* and *CG33543* are unknown. *Obp22a* encodes an odorant binding protein, while *Npc2a* encodes the Niemann-Pick type C-2a protein which is involved sterol homeostasis. The other boundary (purple: indicated by purple arrow) is located between two TADs 2.8 Mb away at 4,794,250 bp. The upstream TAD contains the *fipi* gene (*CG15630*) which has neuronal functions in male courtship, while the downstream TAD contains *CG3294*, which is thought to be a spliceosome component, and *schlaff* (*slf*) which encodes a chitin binding protein. As illustrated in the accompanying diagram, the blue boundary pairs with the purple boundary in a head-to-head orientation, generating a ~2.8 Mb loop with a circle-loop topology. As a result of this pairing, the multi-gene (*CG33543*, *Obp22a* and *Npc2a*) TAD upstream of the blue boundary interacts with the *CG15630* TAD upstream of the purple boundary. Conversely the small *Nplp4:CG15353* TAD downstream of the blue boundary interacts with the *CG3294:slf* TAD downstream of the purple boundary. Even if one imagined that the cohesin bolo tie clip was somehow able to extrude 2.8 Mb of chromatin and then know to stop when it encountered the blue and purple boundaries, it would've generated a stemloop, not a circle-loop.

The second meta-loop (panel B) is more complicated as it is generated by pairing interactions between four boundary elements. The blue boundary (blue arrow) located ~4,801,800 bp (3L) separates a large TAD containing the *RhoGEF64C* gene from a small TAD containing *CG7509*, which encodes a predicted subunit of an extracellular carboxypeptidase. As can be seen in the MicroC contact profile and the accompanying diagram, the blue boundary pairs with the purple boundary (purple arrow) which is located at ~7,013, 500 (3L) just upstream of the 2nd internal promoter (indicated by black arrowhead) of the *Mp* (*Multiplexin*) gene. This pairing interaction is head-to-tail and generates a large stem-loop that spans ~2.2 Mb. The stem-loop brings sequences upstream of the blue boundary and downstream of the purple boundary into contact (the strings below a bolo tie clip), just as was observed in the boundary bypass experiments of Muravyova et al. (Muravyova et al. 2001) and Kyrchanova et al. (Kyrchanova et al. 2008). The physical interactions result in a box of contacts (right top) between sequences in the large *RhoGEF64C* TAD and sequences in a large TAD that contains an internal *Mp* promoter. The second pairing interaction is between the brown boundary (brown arrow) and the green boundary (green arrow). The brown boundary is located at ~4 805,600 bp (3L) and separates the TAD containing *CG7590* from a large TAD containing *CG1808* (predicted to encode an oxidoreductase) and the *Dhc64C* (*Dynein heavy chain 64C*) gene. The green boundary is located at ~6,995,500 bp (3L), and it separates a TAD containing *CG32388* and the *biniou* (*bin*) transcription factor from a TAD that contains the most distal promoter of the *Mp* (*Multiplexin*) gene (blue arrowhead). As indicated in the diagram, the brown and green boundaries pair with each other head-to-tail, and this generates a small internal loop (and the final configuration would resemble a bolo tie with two tie clips). This small internal loop brings the *CG7590* TAD into contact with the TAD that extends from the distal *Mp* promoter to the 2nd internal *Mp* promoter. The resulting contact profile is a rectangular box with diagonal endpoints corresponding to the paired blue:purple and brown:green boundaries. The pairing of the brown:green boundaries also brings the TADs immediately downstream of the brown boundary and upstream of the green boundary into contact with each other, and this gives a rectangular box of interactions between the *Dhc64C* TAD, and sequences in the *bin*/*CG3238* TAD. This box is located on the lower left side of the contact map.

Since the *bin* and *Mp* meta-loops in Author response image 3B are stem-loops, they could have been generated by "sequential" cohesin loop extrusion events. Besides the fact that cohesin extrusion of 2 Mb of chromatin and breaking through multiple intervening TAD boundaries challenges the imagination, there is no mechanism in the cohesion loop

extrusion/CTCF roadblock model to explain why cohesion complex 1 would come to a halt at the purple boundary on one side and the blue boundary on the other, while cohesin complex 2 would instead stop when it hits the brown and green boundaries. This highlights another problem with the cohesin loop extrusion/CTCF roadblock model, namely that the roadblocks are *functionally autonomous*: they have an intrinsic ability to block cohesin that is entirely independent of the intrinsic ability of other roadblocks in the neighborhood. As a result, there is no mechanism for generating specificity in loop formation. By contrast, boundary pairing interactions are by definition non-autonomous and depend on the ability of individual boundaries to pair with other boundaries: specificity is built into the model. The mechanism for pairing, and accordingly the basis for partner preferences/specificity, are reasonably well understood. Probably the most common mechanism in flies is based on shared binding sites for architectural proteins that can form dimers or multimers (Bonchuk et al. 2021; Fedotova et al. 2017). Flies have a large family of polydactyl zinc finger DNA binding proteins, and as noted above, many of these form dimers or multimers and also function as TAD boundary proteins. This pairing principle was first discovered by Kyrchanova et al. (Kyrchanova et al. 2008). This paper also showed that orientation-dependent pairing interactions is a common feature of endogenous fly boundaries. Another mechanism for pairing is specific protein:protein interactions between different DNA binding factors (Blanton et al. 2003). Yet a third mechanism would be proteins that bridge different DNA binding proteins together. The boundaries that use these different mechanisms (BX-C boundaries, *scs*, *scs'*) depend upon the same sorts of proteins that are used by *homie* and *nhomie*. Likewise, these same set of factors reappear in one combination or another in most other TAD boundaries. As for the orientation of pairing interactions, this is most likely determined by the order of binding sites for chromosome architectural proteins in the partner boundaries.

> *…and many TADs lack focal 3D interactions between their boundaries.*

(1.3) The idea that flies differ from mammals in that they "lack" focal 3D interactions is simply mistaken. One of the problems with drawing this distinction is that most all of the "focal 3D interactions" seen mammalian Hi-C experiments are a consequence of binning large DNA segments in low resolution restriction enzyme-dependent experiments. This is even true in the two "high" resolution MicroC experiments that have been published (Hsieh et al. 2020; Krietenstein et al. 2020). As illustrated above in Author response image 1, most of the "focal 3D interactions" (the dots at the apex of TAD triangles) seen with large bin sizes (1 kb and greater) disappear when the bin size is 200 bp and TADs rather than TAD neighborhoods are being visualized.

As described in point #1.1, in the MicroC protocol, fixed chromatin is first digested to mononucloesomes by extensive MNase digestion, processed/biotinylated, and ligated to give dinucleosome-length fragments, which are then sequenced. Regions of chromatin that are nucleosome free (promoters, enhancers, silencers, boundary elements) will typically be reduced to oligonucleotides in this procedure and will not be recovered when dinucleosome-length fragments are sequenced. The loss of sequences from typical paired boundary elements is illustrated by the *lar* meta-loop shown in Author response image 4 (at 200 bp resolution). Panels A and B show the contact profiles generated when the blue boundary (which separates two TADs that span the *Lar* (*Leukocyteantigen-related-like*) transcription unit interacts with the purple boundary (which separates two TADs in a gene poor region ~620 kb away). The blue and purple boundaries pair with each other head-to-head, and this pairing orientation generates yet another circle-loop. In the circle-loop topology, sequences in the TADs upstream of both boundaries come into contact with each other, and this gives the small dark rectangular box to the upper left of the paired boundaries (Author response image 4A). (Note that this small box corresponds to the two small TADs upstream of the blue and purple boundaries, respectively. See panel B.) Sequences in the TADs downstream of the two

boundaries also come into contact with each other, and this gives the large box to the lower right of the paired boundaries. While this meta-loop is clearly generated by pairing interactions between the blue and purple boundaries, the interacting sequences are degraded in the MicroC protocol, and sequences corresponding to the blue and purple boundaries aren't recovered. This can be seen in panel B (red arrow and red arrowheads). When a different Hi-C procedure is used (dHS-C) that captures nucleosome-free regions of chromatin that are physically linked to each other (Author response image 4C & D), the sequences in the interacting blue and purple boundaries are recovered and generate a prominent "dot" at their physical intersection (blue arrow in panel D).

Author response image 4.

Lar metaloop. Panels A & bB: MicroC. Panels C & D: dHS-C

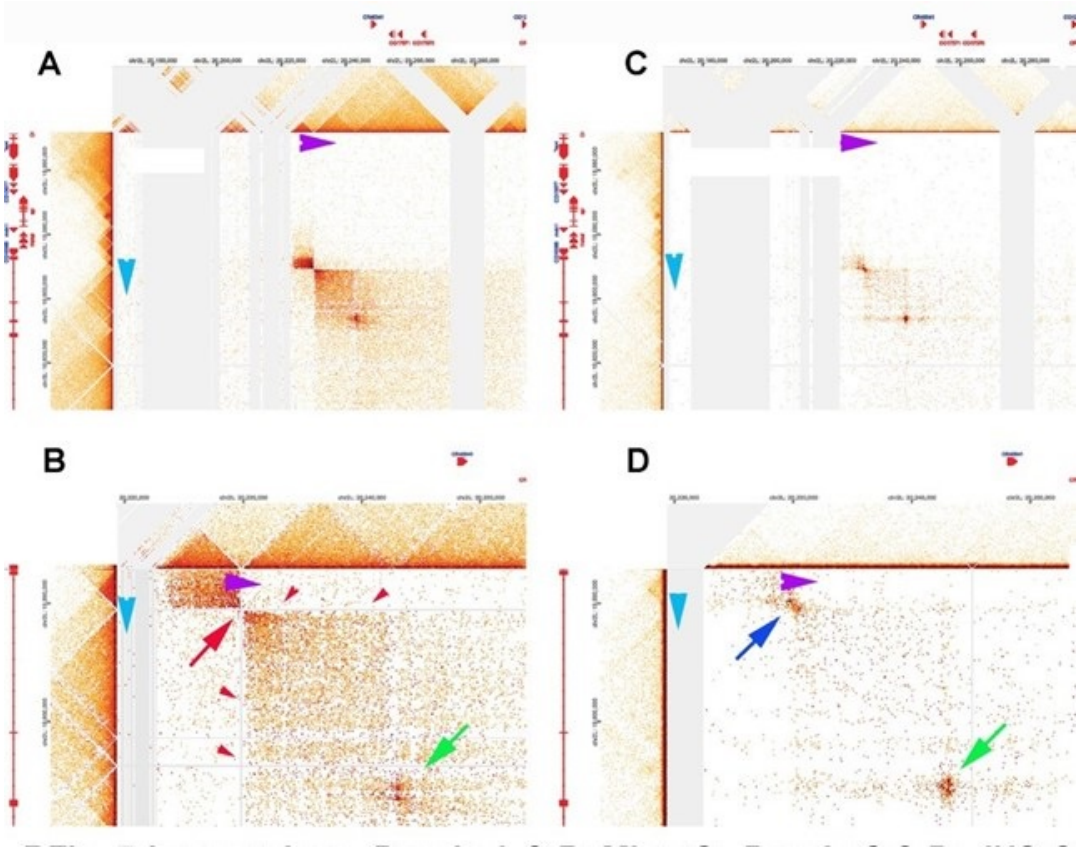

While sequences corresponding to the blue and purple boundaries are lost in the MicroC procedure, there is at least one class of elements that engage in physical pairing interactions whose sequences are (comparatively) resistant to MNase digestion. This class of elements includes many PREs ((Kyrchanova et al. 2018); unpublished data), the boundary bypass elements in the *Abd-B* region of BX-C (Kyrchanova et al. 2023; Kyrchanova et al. 2019a; Kyrchanova et al. 2019b; Postika et al. 2018), and "tethering" elements (Batut et al. 2022; Li et al. 2023). In all of the cases tested, these elements are bound in nuclear extracts by a large (>1000 kD) GAGA factor-containing multiprotein complex called LBC. LBC also binds to the *hsp70* and *eve* promoters (unpublished data). Indirect end-labeling experiments (Galloni et al. 1993; Samal et al. 1981; Udvardy and Schedl 1984) indicate that the LBC protects a ~120-180 bp DNA segment from MNase digestion. It is likely that this is the reason why LBC-bound sequences can be recovered in MicroC experiments as dots when they are physically linked to each other. One such example (based on the ChIP signatures of the paired elements) is indicated by the green arrow in panel B and D of Author response image 4. Note that there

are no dots corresponding to these two LBC elements within either of the TADs immediately downstream of the blue and purple boundaries. Instead the sequences corresponding to the two LBC elements are only recovered when the two elements pair with each other over a distance of ~620 kb. The fact that these two elements pair with each other is consistent with other findings which indicate that, like classical boundaries, LBC elements exhibit partner preferences. In fact, LBC elements can sometimes function as TAD boundaries. For example, the *Fab-7* boundary has two LBC elements, and full *Fab-7* boundary function can be reconstituted with just these two elements (Kyrchanova et al. 2018).

> ***Reviewer #2 (Public Review):***
>
> *"Chromatin Structure II: Stem-loops and circle-loops" by Ke*, Fujioka*, Schedl, and Jaynes reports a set of experiments and subsequent analyses focusing on the role of Drosophila boundary elements in shaping 3D genome structure and regulating gene expression. The authors primarily focus on the region of the fly genome containing the even skipped (eve) gene; eve is expressed in a canonical spatial pattern in fly embryos and its locus is flanked by the well-characterized neighbor of homie (nhomie) and homie boundary elements. The main focus of investigation is the orientation dependence of these boundary elements, which had been observed previously using reporter assays. In this study, the authors use Crispr/Cas9 editing followed by recombination-mediated cassette exchange to create a series of recombinant fly lines in which the nhomie boundary element is either replaced with exongenous sequence from phage λ, an inversion of nhomie, or a copy of homie that has the same orientation as the endogenous homie sequence. The nhomie sequence is also regenerated in its native orientation to control for effects introduced by the transgenesis process.*
>
> *The authors then perform high-resolution Micro-C to analyze 3D structure and couple this with fluorescent and colorimetric RNA in situ hybridization experiments to measure the expression of eve and nearby genes during different stages of fly development. The major findings of these experiments are that total loss of boundary sequence (replacement with λ DNA) results in major 3D structure changes and the most prominent observed gene changes, while inversion of the nhomie boundary or replacement with homie resulted in more modest effects in terms of 3D structure and gene expression changes and a distinct pattern of gene expression change from the λ DNA replacement. As the samples in which the nhomie boundary is inverted or replaced with homie have similar Micro-C profiles at the eve locus and show similar patterns of a spurious gene activation relative to the control, the observed effects appear to be driven by the relative orientation of the nhomie and homie boundary elements to one another.*
>
> *Collectively, the findings reported in the manuscript are of broad interest to the 3D genome field. Although extensive work has gone into characterizing the patterns of 3D genome organization in a whole host of species, the underlying mechanisms that structure genomes and their functional consequences are still poorly understood. The perhaps best understood system, mechanistically, is the coordinated action of CTCF with the cohesin complex, which in vertebrates appears to shape 3D contact maps through a loop extrusion-pausing mechanism that relies on orientation-dependent sequence elements found at the boundaries of interacting chromatin loops.*

(2.1) The notion that mammalian genome is shaped in 3D by the coordinate action of cohesin and CTCF has achieved the status of dogma in the field of chromosome structure in vertebrates. However, as we have pointed out in #1.1, the evidence supporting this dogma is far from convincing. To begin with, it is based on low resolution Hi-C experiments that rely on large bin sizes to visualize so-called “TADs.” In fact, the notion that cohesin/CTCF are responsible on their own for shaping the mammalian 3D genome appears to be a result of mistaking a series of forests for the actual trees that populate each of the forests.

As illustrated in Author response image 1 above, the “TADs” that are visualized in these low resolution data sets are not TADs at all, but rather TAD neighborhoods consisting of several dozen or more individual TADs. Moreover, the “interesting” features that are evident at low resolution (>1 kb)—the dots and stripes—largely disappear at resolutions appropriate for visualizing individual TADs (~200 bp).

In Goel et al. 2023, we presented data from one of the key experiments in Goel et al. (Goel et al. 2023). In this experiment, the authors used RCMC to generate high resolution (~250 bp) MicroC contact maps before and after Rad21 depletion. Contrary to dogma, Rad21 depletion has absolutely no effect on TADs in a ~250 kb DNA segment—and these TADs look very much like the TADs we observe in the *Drosophila* genome, in particular in the *Abd-B* region of BX-C that is thought to be assembled into a series of circle-loops (see Fig. 2B).

While Goel et al. (Goel et al. 2023) observed no effect of Rad21 depletion on TADs, they found that loss of Rad21 disturbs long-distance (but not short-distance) contacts in large TAD neighborhoods when their RCMC data set is visualized using bin sizes of 5 kb and I kb. This is shown in Author response image 2. The significance of this finding is, however, uncertain. It could mean that the 3D organization of large TAD neighborhoods have a special requirement for cohesin activity. On the other hand, since cohesin functions to hold sister chromosomes together after replication until they separate during mitosis (and might also participate in mitotic condensation), it is also possible that the loss of long-range contacts in large TAD neighborhoods when Rad21 is depleted is simply a reflection of this particular activity. Further studies will be required to address these possibilities.

As for CTCF: a careful inspection of the ChIP data in Goel et al. 2023 indicates that CTCF is *not* found at each and every TAD boundary. In fact, the notion that CTCF is the *be-all and end-all* of TAD boundaries in mammals is truly hard to fathom. For one, the demands for specificity in TAD formation (and in regulatory interactions) are likely much greater than those in flies, and specificity can’t be generated by a single DNA binding protein. For another, several dozen chromosomal architectural proteins have already been identified in flies. This means that (unlike what is *thought* to be true in mammals) it is possible to use a combinatorial mechanism to generate specificity in, for example, the long distance interactions in RFig 6 and 7. As noted in #2.1 above, many of the known chromosomal architectural proteins in flies are polydactyl zinc finger proteins (just like CTCF). There are some 200 different polydactyl zinc finger proteins in flies, and the function of only a hand full of these is known at present. However, it seems likely that a reasonable fraction of this class of DNA binding proteins will ultimately turn out to have an architectural function of some type (Bonchuk et al. 2021; Fedotova et al. 2017). The number of different polydactyl zinc finger protein genes in mammals is nearly 3 times that of flies. It is really possible that of these, only CTCF is involved in shaping the 3D structure of the mammalian genome?

> *Despite having a CTCF paralog and cohesin, the Drosophila genome does not appear to be structure by loop extrusion-pausing. The identification of orientation-dependent elements with pronounced structural effects on genome folding thus may shed light on alternative mechanisms used to regulated genome structure, which in turn may yield insights into the significance of particular folding patterns.*

(2.2) Here we would like to draw the reviewer’s and reader’s attention to Author response image 3, which shows that orientation-dependent pairing interactions have a significant impact on physical interactions between different sequences. We would also refer the reader to two other publications. One of these is Kyrchanova et al. (Kyrchanova et al. 2008), which was the first to demonstrate that orientation of pairing interactions matters. The second is Fujioka et al. (Fujioka et al. 2016), which describes experiments indicating that *nhomie* and *homie* pair with each other head-to-tail and with themselves head-to-head.

> *On the whole, this study is comprehensive and represents a useful contribution to the 3D genome field. The transgenic lines and Micro-C datasets generated in the course of the work will be valuable resources for the research community. Moreover, the manuscript, while dense in places, is generally clearly written and comprehensive in its description of the work. However, I have a number of comments and critiques of the manuscript, mainly centering on the framing of the experiments and presentation of the Micro-C results and on manner in which the data are analyzed and reported. They are as follows:*
>
> *Major Points:*
>
> *(1) The authors motivate much of the introduction and results with hypothetical "stem loop" and "circle loop" models of chromosome confirmation, which they argue are reflected in the Micro-C data and help to explain the observed ISH patterns. While such structures may possibly form, the support for these specific models vs. the many alternatives is not in any way justified. For instance, no consideration is given to important biophysical properties such as persistence length, packing/scaling, and conformational entropy. As the biophysical properties of chromatin are a very trafficked topic both in terms of experimentation and computational modeling and generally considered in the analysis of chromosome conformation data, the study would be strengthened by acknowledgement of this body of work and more direct integration of its findings.*

(2.3) The reviewer is not correct in claiming that “stem-loops” and “circle-loops” are “hypothetical.” There is ample evidence that both types of loops are present in eukaryotic genomes, and that loop conformation has significant readouts in terms of not only the physical properties of TADs but also their functional properties. Here we would draw the reviewer’s attention to Author response image 3 and Author response image 4 for examples of loops formed by the orientation-dependent pairing of yet other TAD boundary elements. As evident from the MicroC data in these figures, circle-loops and stem-loops have readily distinguishable contact patterns. The experiments in Fujioka et al. (Fujioka et al. 2016) demonstrate that *homie* and *nhomie* pair with each other head-to-tail, while they pair with themselves head-to-head. The accompany paper (Bing et al. 2024) also provides evidence that loop topology is reflected both in the pattern of activation of reporters and in the MicroC contact profiles. We would also mention again Kyrchanova et al. (Kyrchanova et al. 2008), who were the first to report orientation-dependent pairing of endogenous fly boundaries.

At this juncture it would premature to try to incorporate computational modeling of chromosome conformation in our studies. The reason is that the experimental foundations that would be essential for building accurate models are lacking. As should be evident from RFigs. 1-3 above, studies on mammalian chromosomes are simply not of high enough resolution to draw firm conclusions about chromosome conformation: in most studies only the forests are visible. While the situation is better in flies, there are still too many unknown. As just one example, it would be important to know the orientation of the boundary pairing interactions that generate each TAD. While it is possible to infer loop topology from how TADs interact with their neighbors (a plume versus clouds), a conclusive identification of stem- and circle-loops will require a method to unambiguously determine whether a TAD boundary pairs with its neighbor head-to-head or headto-tail.

> *(2) Similar to Point 1, while there is a fair amount of discussion of how the observed results are or are not consistent with loop extrusion, there is no discussion of the biophysical forces that are thought to underly compartmentalization such as block-polymer co-segregation and their potential influence. I found this absence surprising, as it is generally accepted that A/B compartmentalization essentially can explain the contact maps observed in Drosophila and other non-vertebrate eukaryotes (Rowley, ..., Corces*

> *2017; PMID 28826674). The manuscript would be strengthened by consideration of this phenomenon.*

(2.4) Compartments in mammals have typically been identified and characterized using lowresolution data sets, and these studies have relied on visualizing compartments using quite large bin sizes (>>1 kb). Our experiments have nothing to do with the large-scale compartments seen in these Hi-C experiments. Instead, we are studying the properties of individual TADs: how TADs are formed, the relationship between TAD topology and boundary:boundary pairing, and the impact of TAD topology on interactions between TADs in the immediate neighborhood. There is no evidence to date that these large compartments or "block polymer co-segregation" have a) any impact on the properties of individual boundary elements, b) have a role in determining which boundary elements actually come together to form a given TAD, c) impact the orientation of the interactions between boundaries that generate the TAD or d) determine how TADs tend to interact with their immediate neighbors.

In more recent publications (c.f., Harris et al. 2023) compartments have shrunk in size and instead of being units of several hundred kb, the median length of the "compartmental" unit in mammalian cells is about12 kb. This is not too much different from the size of fly TADs. However, the available evidence does not support the idea that block polymer co-segregation/co-repulsion drive the TAD:TAD interactions seen in MicroC experiments. For example, according to this "micro-compartment" model, the specific patterns of interaction between TADs in the *CG3294* meta-loop in Author response image 3 would be driven by block polymer co-segregation and co-repulsion. In this model, the TAD upstream of the blue boundary (which contains *CG33543*, the odorant binding protein gene *Obp22a* and the *Npc2a* gene which encodes a protein involved in sterol homeostasis) would share the same chromatin state/biophysical properties as the TAD upstream of the purple boundary, which has the *fipi* gene. While it is true that *CG33543*, *Obp22a* and also the *fipi* gene are not expressed in embryos, *Npc2a* is expressed at high levels during embryogenesis, yet it is part of the TAD that interacts with the *fipi* TAD. The TAD downstream of the blue boundary contains *CG15353* and *Nplp4* and it interacts with the TAD downstream of the purple boundary which contains *CG3294* and *slf*. *CG15353* and *Nplp4* are not expressed in the embryo and as such should share a compartment with a TAD that is *also* silent. However, *slf* is expressed at a high level in 1216 hr embryos, while *CG3294* is expressed at a low level. In neither case would one conclude that the TADs upstream and downstream of the blue and purple boundaries, respectively, interact because of shared chromatin/biophysical states that drive block polymer co-segregation corepulsion.

One might also consider several gedanken experiments involving the long-range interactions that generate the *CG3294* meta-loop in Author response image 3. According to the micro-compartment model the patchwork pattern of crosslinking evident in the *CG3294* meta-loop arises because the interacting TADs share the same biochemical/biophysical properties, and this drives block polymer cosegregation and co-repulsion. If this model is correct, then this patchwork pattern of TAD:TAD interactions would remain unchanged if we were to delete the blue or the purple boundary. However, given what we know about how boundaries can find and pair with distant boundaries (c.f., Figure 6 from Muller et el. 1999 and the discussion in #1.2), the result of these gedanken experiments seem clear: the patchwork pattern shown in Author response image 3A will disappear. What would happen if we inverted the blue or the purple boundary? Would the TAD containing *CG33543*, *Obp22a* and *Npc2a* still interact with *fipi* as would be expected from the compartment model? Or would the pattern of interactions flip so that the *CG33543*, *Obp22a* and *Npc2a* TAD interacts with the TAD containing *CG3294* and *slf*? Again we can anticipate the results based on previous studies: the interacting TADs will switch when the *CG3294* meta-loop is converted into a stem-loop. If this happened, the only explanation possible in the compartment model is that the chromatin states change when the boundary is inverted so that TAD upstream of blue boundary now shares the same chromatin state as the TAD downstream of the purple boundary, while the TAD downstream

of the blue boundary shares same state as the TAD upstream of the purple boundary. However, there is no evidence that boundary orientation per se can induce a complete switch in “chromatin states” as would be required in the compartment model.

While we have not done these experimental manipulations with the *CG3294* meta-loop, an equivalent experiment was done in Bing et al. (Bing et al. 2024). However, instead of deleting a boundary element, we inserted a *homie* boundary element together with two reporters (*gfp* and *LacZ*) 142 kb away from the *eve* TAD. The result of this gedanken “reverse boundary deletion” experiment is shown in Author response image 5. Panel A shows the MicroC contact profile in the region spanning the transgene insertion site and the *eve* TAD in wild type (*read* “deletion”) NC14 embryos. Panel B shows the MicroC contact profile from 12-16 hr embryos carrying the *homie* dual reporter transgene inserted at -142 kb. Prior to the “deletion”, the *homie* element in the transgene pairs with *nhomie* and *homie* in the *eve* TAD and this generates a “mini-metaloop.” In this particular insert, the *homie* boundary in the transgene (red arrow) is “pointing” in the opposite orientation from the *homie* boundary in the *eve* TAD (red arrow). In this orientation, the pairing of the transgene *homie* with *eve nhomie/homie* brings the *LacZ* reporter into contact with sequences in the *eve* TAD. Since a mini-metaloop is formed by *homie*à *nhomie/homie* pairing, sequences in TADs upstream and downstream of the transgene insert interact with sequences in TADs close to the *eve* TAD (Author response image 5B). Taken together these interactions correspond to the interaction patchwork that is typically seen in “compartments” (see boxed region and inset). If this patchwork is driven as per the model, by block polymer co-segregation and co-repulsion, then it should still be present when the transgene is deleted. However, panel A shows that the interactions linking the transgene *and* the sequences in TADs next to the transgene to *eve* and TADs next to *eve* disappear when the *homie* boundary (plus transgene) is “deleted” in wild type flies.

Author response image 5.

Boundary deletion and compartments

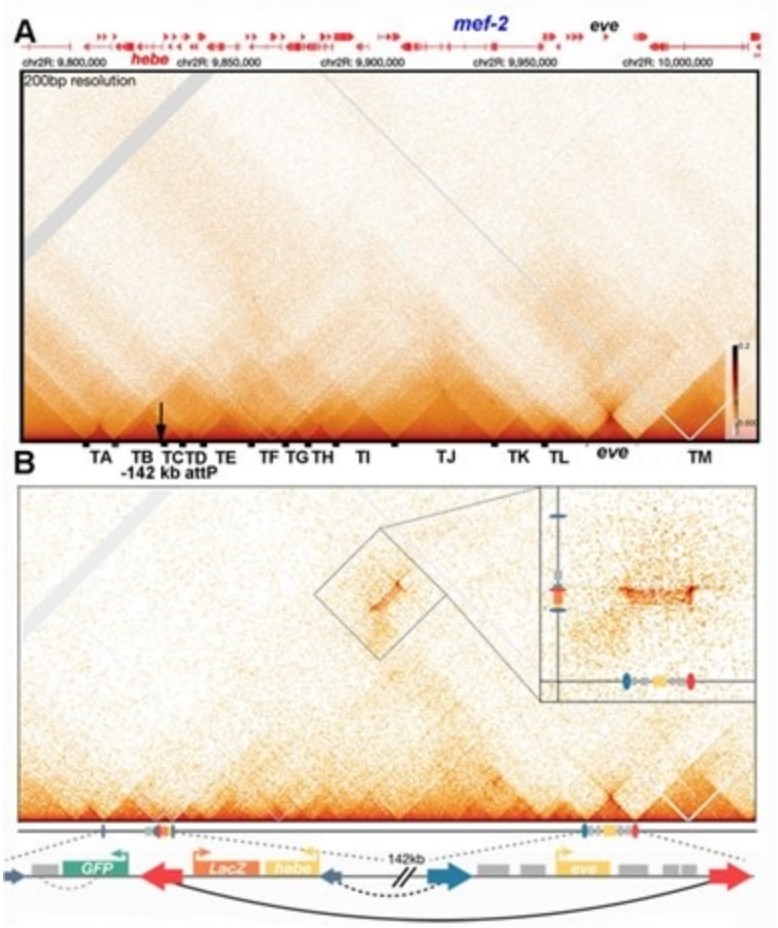

A second experiment would be to invert the *homie* boundary so that instead of pointing away from *eve* it points towards *eve*. Again, if the compartmental patchwork is driven by block polymer co-segregation and co-repulsion, inverting the *homie* boundary in the transgene should have no effect on the compartmental contact profile. Inspection of Fig. 7 in Bing et al. (Bing et al. 2024) will show that this prediction doesn't hold either. When *homie* is inverted, sequences in the *eve* TAD interact with the *gfp* reporter not the *LacZ* reporter. In addition, there are corresponding changes in how sequences in TADs to either side of *eve* interact with sequences to either side of the transgene insert.

Yet another "test" of compartments generated by block polymer co-segregation/co-repulsion is provided by the plume above the *eve* volcano triangle. According to the compartment model, sequences in TADs flanking the *eve* locus form the plume above the *eve* volcano triangle because their chromatin shares properties that drive block polymer co-segregation. These same properties result in repulsive interactions with chromatin in the *eve* TAD, and this would explain why the *eve* TAD doesn't crosslink with its neighbors. If the distinctive chromatin properties of *eve* and the neighboring TADs drive block polymer co-segregation and co-repulsion, then inverting the *nhomie* boundary or introducing *homie* in the forward orientation should have absolutely no effect on the physical interactions between chromatin in the *eve* TAD and chromatin in the neighboring TADs. However, Figures 4 and 6 in this paper indicate that boundary pairing orientation, not block polymer co-segregation/co-repulsion, is responsible for forming the plume above the *eve* TAD. Other findings also appear to be inconsistent with the compartment model. (A) The plume topping the *eve* volcano triangle is present in NC14 embryos when *eve* is broadly expressed (and potentially active throughout the embryo). It is also present in 12-16 hr embryos when *eve* is only expressed in a very small subset of cells and is subject to PcG silencing everywhere else in the embryo. B)

According to the compartment model the precise patchwork pattern of physical interactions should depend upon the transcriptional program/chromatin state that is characteristic of a particular developmental stage or cell type. As cell fate decisions are just being made during NC14 one might expect that most nuclei will share similar chromatin states throughout much of the genome. This would not be true for 12-16 hr embryos. At this stage the compartmental patchwork would be generated by a complex mixture of interactions in cells that have quite different transcriptional programs and chromatin states. In this case, the patchwork pattern would be expected to become fuzzy as a given chromosomal segment would be in compartment A in one group of cells and in compartment B in another. Unlike 12-16 hr embryos, larval wing discs would be much more homogeneous and likely give a distinct and relatively well resolved compartmental pattern. We've examined the compartment patchwork of the same chromosomal segments in NC14 embryos, 12-16 hr embryos and larval wing disc cells. While there are some differences (e.g., changes in some of the BX-C TADs in the wing disc sample) the compartmental patchwork patterns are surprisingly similar in all three cases. Nor is there any "fuzziness" in the compartmental patterns evident in 12-16 hr embryos, despite the fact that there are many different cell types at this stage of development. C) TAD interactions with their neighbors and compartmental patchworks are substantially suppressed in salivary gland polytene chromosomes. This would suggest that features of chromosome structure might be the driving force behind many of the "compartmental" interactions as opposed to distinct biochemical/biophysical of properties of small chromosomal segments that drive polymer co- segregation/co-repulsion.

> *(3) The contact maps presented in the study represent many cells and distinct cell types. It is clear from single-cell Hi-C and multiplexed FISH experiments that chromosome conformation is highly variable even within populations of the same cell, let alone between cell types, with structures such as TADs being entirely absent at the single cell level and only appearing upon pseudobulking. It is difficult to square these observations with the models of relatively static structures depicted here. The authors should provide commentary on this point.*

(2.5) As should be evident from Author response image 1, single-cell Hi-C experiments would not provide useful information about the physical organization of individual TADs, TAD boundaries or how individual TADs interact with their immediate neighbors. In addition, since they capture only a very small fraction of the possible contacts within and between TADs, we suspect that these single-cell studies aren't likely to be useful for making solid conclusions about TAD neighborhoods like those shown in Author response image 1 panels A, B, C and D, or Author response image 2. While it might be possible to discern relatively stable contacts between pairs of insulators in single cells with the right experimental protocol, the stabilities/dynamics of these interactions may be better judged by the length of time that physical interactions are seen to persist in live imaging studies such as Chen et al. (2018), Vazquez et al. (2006) and Li et al. (2011).

The *in situ* FISH data we've seen also seems problematic in that probe hybridization results in a significant decondensation of chromatin. For two probe sets complementary to adjacent ~1.2 kb DNA sequences, the measured center-to-center distance that we've seen was ~110 nM. This is about 1/3rd the length that is expected for a 1.2 kb naked DNA fragment, and about 1.7 times larger than that expected for a beads-on-a-string nucleosome array (~60 nM). However, chromatin is thought to be compacted into a 30 nM fiber, which is estimated to reduce the length of DNA by at least another ~6 fold. If this estimate is correct, FISH hybridization would appear to result in a ~10 fold decompaction of chromatin. A decompaction of this magnitude would necessarily be followed by a significant distortion in the actual conformation of chromatin loops.

> *(4) The analysis of the Micro-C data appears to be largely qualitative. Key information about the number of reads sequenced, reaps mapped, and data quality are not presented. No quantitative framework for identifying features such as the "plumes" is described. The study and its findings would be strengthened by a more rigorous analysis of these rich datasets, including the use of systematic thresholds for calling patterns of organization in the data.*

Additional information on the number of reads and data quality have been included in the methods section.

> *(5) Related to Point 4, the lack of quantitative details about the Micro-C data make it difficult to evaluate if the changes observed are due to biological or technical factors. It is essential that the authors provide quantitative means of controlling for factors like sampling depth, normalization, and data quality between the samples.*

In our view the changes in the MicroC contact patterns for the *eve* locus and its neighbors when the *nhomie* boundary is manipulated are not only clear cut and unambiguous but are also readily evident in the Figs that are presented in the manuscript. If the reviewer believes that there aren't significant differences between the MicroC contact patterns for the four different *nhomie* replacements, it seems certain that they would also remain unconvinced by a quantitative analysis.

The reviewer also suggests that biological and/or technical differences between the four samples could account for the observed changes in the MicroC patterns for the *eve* TAD and its neighbors. If this were the case, then similar changes in MicroC patterns should be observed elsewhere in the genome. Since much of the genome is analyzed in these MicroC experiments there is an abundance of internal controls for each experimental manipulation of the *nhomie* boundary. For two of the *nhomie* replacements, *nhomie reverse* and *homie forward*, the plume above the *eve* volcano triangle is replaced by clouds surrounding the *eve* volcano triangle. If these changes in the *eve* MicroC contact patterns are due to significant technical (or biological) factors, we should observe precisely the same sorts of changes in TADs elsewhere in the genome that are volcano triangles with plumes. Author response image 6 shows the MicroC contact pattern for several genes in the Antennapedia complex. The *deformed* gene is included in a TAD which, like *eve*, is a volcano triangle topped by a plume. A comparison of the *deformed* MicroC contact patterns for *nhomie forward* (panel B) with the MicroC patterns for *nhomie reverse* (panel C) and *homie forward* (panel D) indicates that while there are clearly technical differences between the samples, these differences do not result in the conversion of the *deformed* plume into clouds as is observed for the *eve* TAD. The MicroC patterns elsewhere in Antennapedia complex are also very similar in all four samples. Likewise, comparisons of regions elsewhere in the fly genome indicate that the basic contact patterns are similar in all four samples. So while there are technical differences which are reflected in the relative pixel density in the TAD triangles and the LDC domains, these differences do not result in converting plumes into clouds nor do the alter the basic patterns of TAD triangles and LDC domains. As for biological differences— the embryos in each sample are at roughly the same developmental stage and were collected and processed using the same procedures. Thus, the biological factors that could reasonably be expected to impact the organization of specific TADs (e.g., cell type specific differences) are not going to impact the patterns we see in our experiments.

Author response image 6.

> *(6) The ISH effects reported are modest, especially in the case of the HCR. The details provided for how the imaging data were acquired and analyzed are minimal, which makes evaluating them*

challenging. It would strengthen the study to provide much more detail about the acquisition and analysis and to include depiction of intermediates in the analysis process, e.g. the showing segmentation of stripes.

The imaging analysis is presented in Fig. 5 is just standard confocal microscopy. Individual embryos were visualized and scored. An embryo in which stripes could be readily detected was scored as 'positive' while an embryo in which stripes couldn't be detected was scored as 'negative.'

> ***Recommendations for the authors:***
>
> ***Editor comments:***
>
> *It was noted that the Jaynes lab previously published extensive genetic evidence to support the stem loop and circle loop models of Homie-Nhomie interactions (Fujioka 2016 Plos Genetics) that were more convincing than the Micro-C data presented here in proof of their prior model. Maybe the authors could more clearly summarize their prior genetic results to further try to convince the reader about the validity of their model.*
>
> ***Reviewer #1 (Recommendations For The Authors):***

Below, I list specific comments to further improve the manuscript for publication. Most importantly, I recommend the authors tone down their proposal that boundary pairing is a universal TAD forming mechanism.

(1) The title is cryptic.

(2) The second sentence in the abstract is an overstatement: "In flies, TADs are formed by physical interactions between neighboring boundaries". Hi-C and Micro-C studies have not provided evidence that most TADs in Drosophila show focal interactions between their bracketing boundaries. The authors rely too strongly on prior studies that used artificial reporter transgenes to show that multimerized insulator protein binding sites or some endogenous fly boundaries can mediate boundary bypass, as evidence that endogenous boundaries pair.

Please see responses #1.1 and #1.3 and figures Author response image 1 and Author response image 3. Note that using dHS-C, most TADs that we've looked at so far are topped by a "dot" at their apex.

> *(3) Line 64: the references do not cite the stated "studies dating back to the '90's'".*

The papers cited for that sentence are reviews which discussed the earlier findings. The relevant publications are cited at the appropriate places in the same paragraph.

> *(4) Line 93: "On the other hand, while boundaries have partner preferences, they are also promiscuous in their ability to establish functional interactions with other boundaries." It was unclear what is meant here.*

Boundaries that a) share binding sites for proteins that multimerized, b) have binding sites for proteins that interact with each other, or c) have binding sites for proteins that can be bridged by a third protein can potentially pair with each other. However, while these mechanisms enable promiscuous pairing interactions, they will also generate partner preferences (through a greater number of a, b and/or c).

> *(5) It could be interesting to discuss the fact that it remains unclear whether Nhomie and Homie pair in cis or in trans, given that homologous chromosomes are paired in*

> *Drosophila.*

The studies in Fujioka et al. (Fujioka et al. 2016) show that *nhomie* and *homie* can pair both in *cis* and in *trans*. Given the results described in #1.2, we imagine that they are paired in both *cis* and *trans* in our experiments.

> *(6) Line 321: Could the authors further explain why they think that "the nhomie reverse circle-loop also differs from the nhomie deletion (λ DNA) in that there is not such an obvious preference for which eve enhancers activate expression"?*

The likely explanation is that the topology/folding of the altered TADs impacts the probability of interactions between the various *eve* enhancers and the promoters of the flanking genes.

> *(7) The manuscript would benefit from shortening the long Discussion by avoiding repeating points described previously in the Results.*
>
> *(8) Line 495: "If, as seems likely, a significant fraction of the TADs genome-wide are circle loops, this would effectively exclude cohesin-based loop extrusion as a general mechanism for TAD formation in flies". The evidence provided in this manuscript appears insufficient to discard ample evidence from multiple laboratories that TADs form by compartmentalization or loop extrusion. Multiple laboratories have, for example, demonstrated that cohesin depletion disrupts a large fraction of mammalian TADs.*

Points made here and in #9 have been responded to in #1.1, #2.1 and #2.4 above. We would suggest that the evidence for loop extrusion falls short of compelling (as it is based on the analysis of TAD neighborhoods, not TADs—that is forests, not trees) and given the results reported in Goel et al. (in particular Fig. 4 and Sup Fig. 8) is clearly suspect. This is not to mention the fact that cohesin loop-extrusion can't generate circle-loops TADs, yet circle-loops clearly exist. Likewise, as discussed in #2.4, it is not clear to us that the shared chromatin states, polymer co-segregation and co-repulsion account for the compartmental patchwork patterns of TAD;TAD interactions. The results from the experimental manipulations in this paper and the accompanying paper, together with studies by others (e.g., Kyrchanova et al. (Kyrchanova et al. 2008), Mohana et al. (Mohana et al. 2023) would also seem to be at odds with the model for compartments as currently formulated.

> *The unique properties of Nhomie and Homie, namely the remarkable specificity with which they physically pair over large distances (Fujioka et al. 2016) may rather suggest that boundary pairing is a phenomenon restricted to special loci. Moreover, it has not yet been demonstrated that Nhomie or Homie are also able to pair with the TAD boundaries on their left or right, respectively.*

Points made here were discussed in detail in #1.2. As described in detail in #1.2, It is not the case that *nhomie* and *homie* are in "unique" or "special." Other fly boundaries can do the same things. As for whether *nhomie* and *homie* pair with their neighbors: We haven't done transgene experiments (e.g., testing by transvection or boundary bypass). Likewise, in MicroC experiments there are no obvious dots at the apex of the neighboring TADs that would correspond to *nhomie* pairing with the neighboring boundary to the left and *homie* pairing with the neighboring boundary to the right. However, this is to be expected. As we discussed in in #1.3 above, only MNase resistant elements will generate dots in standard MicroC experiments. On the other hand, when boundary:boundary interactions are analyzed by dHS-C (c.f., Author response image 4), there are dots at the apex of both neighboring TADs. This would be direct evidence that *nhomie* pairs with the neighboring boundary to the left and *homie* pairs with the neighboring boundary to the right.

> *(9) The comment in point 8 also applies to the concluding 2 sentences (lines 519-524) of the Discussion.*

See response to 8 above. Otherwise, the concluding sentences are completely accurate. Validation of the cohesin loop extrusion/CTCF roadblock model will required demonstrating a) that all TADs are either stem-loops or unanchored loops and b) that TAD endpoints are always marked by CTCF.

The likely presence of circle-loops and evidence that TAD boundaries that don't have CTCF (c.f.,Goel et al. 2023) already suggests that this model can't (either fully or not all) account for TAD formation in mammals.

> *(10) Figs. 3 and 6: It would be helpful to add the WT screenshot in the same figure, for direct comparison.*

It is easy enough to scroll between Figs-especially since *nhomie forward* looks just like WT.

> *(11) Fig. 6: It would be helpful to show a cartoon view of a circle loop to the right of the Micro-C screenshot, as was done in Fig. 3.*

Good idea. Added to the Fig.

> *(12) Fig. 5: It would be helpful to standardize the labelling of the different genotypes throughout the figures and panels ("inverted" versus "reverse" versus an arrow indicating the direction).*

Fixed.

> ***Reviewer #2 (Recommendations For The Authors):***
>
> *Minor Points:*
>
> *(1) The Micro-C data does not appear to be deposited in an appropriate repository. It would be beneficial to the community to make these data available in this way.*

This has been done.

> *(2) Readers not familiar with Drosophila development would benefit from a gentle introduction to the stages analyzed and some brief discussion on how the phenomenon of somatic homolog pairing might influence the study, if at all.*

We included a rough description the stages that were analyzed for both the in situs and MicroC. We thought that an actual description of what is going on at each of the stages wasn't necessary as the process of development is not a focus of this manuscript. In other studies, we've found that there are only minor differences in MicroC patterns between the blastoderm stage and stage 12-16 embryos. While these minor differences are clearly interesting, we didn't discuss them in the text. In all of experiments chromosomes are likely to be paired. In NC14 embryos (the stage for visualizing *eve* stripes and the MicroC contact profiles in Fig. 2) replication of euchromatic sequences is thought to be quite rapid. While homolog pairing is incomplete at this stage, sister chromosomes are paired. In stage 12-16 embryos, homologs will be paired and if the cells are arrested in G2, then sister chromosome will also be paired. So in all of experiments, chromosomes (sisters and/or homologs) are paired. However, since we don't have examples of unpaired chromosomes, our experiments

don’t provide any info on how chromosome pairing might impact MicroC/expression patterns.

> *(3) "P > 0.01" appears several times. I believe the authors mean to report "P < 0.01".*

Fixed.

References for Response

Batut PJ, Bing XY, Sisco Z, Raimundo J, Levo M, Levine MS. 2022. Genome organization controls transcriptional dynamics during development. Science. 375(6580):566-570.

Bing X, Ke W, Fujioka M, Kurbidaeva A, Levitt S, Levine M, Schedl P, Jaynes JB. 2024. Chromosome structure i: Loop extrusion or boundary:Boundary pairing? eLife.

Blanton J, Gaszner M, Schedl P. 2003. Protein:Protein interactions and the pairing of boundary elements in vivo. Genes Dev. 17(5):664-675.

Bonchuk A, Boyko K, Fedotova A, Nikolaeva A, Lushchekina S, Khrustaleva A, Popov V, Georgiev P. 2021. Structural basis of diversity and homodimerization specificity of zincfinger-associated domains in drosophila. Nucleic Acids Res. 49(4):2375-2389.

Bonchuk A, Kamalyan S, Mariasina S, Boyko K, Popov V, Maksimenko O, Georgiev P. 2020. Nterminal domain of the architectural protein ctcf has similar structural organization and ability to self-association in bilaterian organisms. Sci Rep. 10(1):2677.

Chen H, Levo M, Barinov L, Fujioka M, Jaynes JB, Gregor T. 2018. Dynamic interplay between enhancer–promoter topology and gene activity. Nat Genet. 50(9):1296.

Fedotova AA, Bonchuk AN, Mogila VA, Georgiev PG. 2017. C2h2 zinc finger proteins: The largest but poorly explored family of higher eukaryotic transcription factors. Acta Naturae. 9(2):47-58.

Fujioka M, Ke W, Schedl P, Jaynes JB. 2024. The homie insulator has sub-elements with different insulating and long-range pairing properties. bioRxiv. 2024.02.01.578481.

Fujioka M, Mistry H, Schedl P, Jaynes JB. 2016. Determinants of chromosome architecture: Insulator pairing in *cis* and in *trans*. PLoS Genet. 12(2):e1005889.

Galloni M, Gyurkovics H, Schedl P, Karch F. 1993. The bluetail transposon: Evidence for independent cis-regulatory domains and domain boundaries in the bithorax complex. The EMBO Journal. 12(3):1087-1097.

Gaszner M, Vazquez J, Schedl P. 1999. The zw5 protein, a component of the scs chromatin domain boundary, is able to block enhancer-promoter interaction. Genes Dev. 13(16):2098-2107.

Goel VY, Huseyin MK, Hansen AS. 2023. Region capture micro-c reveals coalescence of enhancers and promoters into nested microcompartments. Nat Genet. 55(6):1048-1056.

Harris HL, Gu H, Olshansky M, Wang A, Farabella I, Eliaz Y, Kalluchi A, Krishna A, Jacobs M, Cauer G et al. 2023. Chromatin alternates between a and b compartments at kilobase scale for subgenic organization. Nat Commun. 14(1):3303.

Hart CM, Zhao K, Laemmli UK. 1997. The scs' boundary element: Characterization of boundary element-associated factors. Mol Cell Biol. 17(2):999-1009.

Hsieh TS, Cattoglio C, Slobodyanyuk E, Hansen AS, Rando OJ, Tjian R, Darzacq X. 2020. Resolving the 3d landscape of transcription-linked mammalian chromatin folding. Mol Cell.

78(3):539-553.e538.

Krietenstein N, Abraham S, Venev SV, Abdennur N, Gibcus J, Hsieh TS, Parsi KM, Yang L, Maehr R, Mirny LA et al. 2020. Ultrastructural details of mammalian chromosome architecture. Mol Cell. 78(3):554-565.e557.

Kyrchanova O, Chetverina D, Maksimenko O, Kullyev A, Georgiev P. 2008. Orientation-dependent interaction between drosophila insulators is a property of this class of regulatory elements. Nucleic Acids Res. 36(22):7019-7028.

Kyrchanova O, Ibragimov A, Postika N, Georgiev P, Schedl P. 2023. Boundary bypass activity in the abdominal-b region of the drosophila bithorax complex is position dependent and regulated. Open Biol. 13(8):230035.

Kyrchanova O, Kurbidaeva A, Sabirov M, Postika N, Wolle D, Aoki T, Maksimenko O, Mogila V, Schedl P, Georgiev P. 2018. The bithorax complex iab-7 polycomb response element has a novel role in the functioning of the fab-7 chromatin boundary. PLoS Genet. 14(8):e1007442.
Kyrchanova O, Sabirov M, Mogila V, Kurbidaeva A, Postika N, Maksimenko O, Schedl P, Georgiev P. 2019a. Complete reconstitution of bypass and blocking functions in a minimal artificial fab-7 insulator from drosophila bithorax complex. Proceedings of the National Academy of Sciences.201907190.

Kyrchanova O, Wolle D, Sabirov M, Kurbidaeva A, Aoki T, Maksimenko O, Kyrchanova M, Georgiev P, Schedl P. 2019b. Distinct elements confer the blocking and bypass functions of the bithorax fab-8 boundary. Genetics.genetics. 302694.302019.

Kyrchanova O, Zolotarev N, Mogila V, Maksimenko O, Schedl P, Georgiev P. 2017. Architectural protein pita cooperates with dctcf in organization of functional boundaries in bithorax complex. Development. 144(14):2663-2672.

Li H-B, Muller M, Bahechar IA, Kyrchanova O, Ohno K, Georgiev P, Pirrotta V. 2011. Insulators, not polycomb response elements, are required for long-range interactions between polycomb targets in drosophila melanogaster. Mol Cell Biol. 31(4):616-625.

Li X, Tang X, Bing X, Catalano C, Li T, Dolsten G, Wu C, Levine M. 2023. Gaga-associated factor fosters loop formation in the drosophila genome. Mol Cell. 83(9):1519-1526.e1514.

Mohana G, Dorier J, Li X, Mouginot M, Smith RC, Malek H, Leleu M, Rodriguez D, Khadka J, Rosa P et al. 2023. Chromosome-level organization of the regulatory genome in the drosophila nervous system. Cell. 186(18):3826-3844.e3826.

Muller M, Hagstrom K, Gyurkovics H, Pirrotta V, Schedl P. 1999. The mcp element from the drosophila melanogaster bithorax complex mediates long-distance regulatory interactions. Genetics. 153(3):1333-1356.

Muravyova E, Golovnin A, Gracheva E, Parshikov A, Belenkaya T, Pirrotta V, Georgiev P. 2001. Loss of insulator activity by paired su(hw) chromatin insulators. Science. 291(5503):495498.

Postika N, Metzler M, Affolter M, Müller M, Schedl P, Georgiev P, Kyrchanova O. 2018. Boundaries mediate long-distance interactions between enhancers and promoters in the drosophila bithorax complex. PLoS Genet. 14(12):e1007702.

Samal B, Worcel A, Louis C, Schedl P. 1981. Chromatin structure of the histone genes of d. Melanogaster. Cell. 23(2):401-409.

Sigrist CJ, Pirrotta V. 1997. Chromatin insulator elements block the silencing of a target gene by the drosophila polycomb response element (pre) but allow trans interactions between pres on different chromosomes. Genetics. 147(1):209-221.

Udvardy A, Schedl P. 1984. Chromatin organization of the 87a7 heat shock locus of drosophila melanogaster. J Mol Biol. 172(4):385-403.

Vazquez J, Muller M, Pirrotta V, Sedat JW. 2006. The mcp element mediates stable long-range chromosome-chromosome interactions in drosophila. Molecular Biology of the Cell. 17(5):2158-2165.

Zolotarev N, Fedotova A, Kyrchanova O, Bonchuk A, Penin AA, Lando AS, Eliseeva IA, Kulakovskiy IV, Maksimenko O, Georgiev P. 2016. Architectural proteins pita, zw5,and zipic contain homodimerization domain and support specific long-range interactions in drosophila. Nucleic Acids Res. 44(15):7228-7241.

https://doi.org/10.7554/eLife.94114.2.sa3